DETECTING LANDSCAPE RESPONSE TO PERTURBATIONS BY ^{10}Be AND ^{26}Al
IN CENTRAL PENNSYLVANIA

A Thesis Presented

by

Alison Denn

to

The Faculty of the Graduate College

of

The University of Vermont

In Partial Fulfillment of the Requirements
for the Degree of Master of Science
Specializing in Geology

May 2017

Defense Date: March 8th, 2017
Thesis Examination Committee:

Paul R. Bierman, Ph.D., Advisor
Shelly A. Rayback, Ph.D., Chairperson
Julia N. Perdrial, Ph.D.

ABSTRACT

The change of topography with time and the consequent structure of Earth's surface is dependent on the production and transport of weathered bedrock. I use measurements of *in-situ* cosmogenic ^{10}Be to investigate erosion rates and exposure ages of boulders, streams, and hillslope sediments in central Pennsylvania, a landscape shaped by glacial/interglacial climate cycles and changes in base level. I measure rates of landscape change at three separate sites, Hickory Run boulder field, Young Womans Creek watershed, and Garner Run, a small upland catchment bounded by two ridgelines.

Hickory Run Boulder field is the largest of its kind in the eastern United States. This enigmatic, 1-km-long field of boulders has been attributed to frost-induced processes during the last glacial maximum, when the Laurentide ice sheet margin was nearby. My isotopic data demonstrate that Hickory Run, and likely many other similar boulder fields in eastern North America are ancient, multigenerational features that have persisted over many glacial-interglacial cycles. These findings add nuance to the conventional view of periglaciation as a force that 'wiped the slate clean' in the Appalachian Mountains—in upland areas with resistant lithologies, I show that the landscape was reworked, but not reset by repeated periglaciation.

Young Womans Creek is a 230 km^2 drainage basin in the headwaters of the Appalachian Plateau physiographic province, where I investigate the role of non-equilibrium topography on the rates of erosion at a basin scale. Here, I use *in-situ* ^{10}Be to understand the influence of fluvial incision into the landscape, contrasting erosion rates in undissected uplands with those in incised valleys. Erosion rates are positively correlated with slope, but correlate negatively with normalized channel steepness, k_{sn}, and downstream distance. My results demonstrate the effects of lithology and base level on erosion rate are difficult to disentangle, and that when studied on a small scale, lithology exerts the strongest control over the spatial variability of erosion in a transient landscape.

Resistant sandstone ridgelines such as those at Garner Run are common features in the Ridge and Valley province of central Pennsylvania. At this site, I strive to understand the influence of periglacial activity on the generation and movement of sediment downslope. My measurements demonstrate that sediment in small upland catchments such as Garner Run can have cosmogenic nuclide concentrations equal to and exceeding 100,000 years of surface exposure history. Despite perturbations by multiple glacial/interglacial cycles throughout the Pleistocene these sandstone-underlain environments are not young, and the exposure of surficial materials predates the last major advance of the Laurentide Ice Sheet at ~26,000 years ago.

ACKNOWLEDGEMENTS

> *Did I fall in love here once?*
> *Or was I young here once?*
> *Oh, whatever the reason this place feels like home to me.*

TABLE OF CONTENTS

LIST OF TABLES

CHAPTER 3: BEDROCK MATTERS: LITHOLOGIC CONTROL OF EROSION RATES OVERWHELMS EFFECT OF BASE LEVEL FALL

CHAPTER 4: GARNER RUN

LIST OF FIGURES

CHAPTER 2: A HALF-MILLION YEAR OLD FOSSIL LANDFORM IN CENTRAL PENNSYLVANIA

CHAPTER 3: BEDROCK MATTERS: LITHOLOGIC CONTROL OF EROSION RATES OVERWHELMS EFFECT OF BASE LEVEL FALL

CHAPTER 4: GARNER RUN

CHAPTER 1: INTRODUCTION

1.1 Motivation and overview

The landscape in Pennsylvania is complex, and is the product of many different forcings over geologic time. Located in the heart of the Appalachian mountain range, Pennsylvania marks the furthest southern extent of the Laurentide ice sheet in the northeastern United States (Braun, 1989; Sevon, 2000). Over millions of years orogeny has formed resistant quartzite ridgelines and limestone valleys. On timescales of thousands to hundreds of thousands of years the region has been sculpted by glacial/interglacial cycles and the incision of rivers into the landscape. My research focuses on these 'shorter' timescales, and examines the ages and erosion rates of surficial materials south of the last glacial maximum boundary in Pennsylvania.

This project is a cosmogenic isotopic investigation of rates of landscape change in in which I use *in-situ* ^{10}Be and ^{26}Al to measure erosion rates and to estimate residence times of boulders, soils, and fluvial sediment. My thesis is comprised of three separate projects. The first chapter describes my work at Hickory Run State Park, where I use cosmogenic nuclides to infer effective exposure ages of boulders in an enigmatic, nearly flat boulder field that was likely formed in part by periglacial processes at past glacial maxima. The second chapter shifts away from climate to investigate the role of lithology and fluvial incision on erosion rates in a small watershed in the Appalachian Plateau, Young Womans Creek. In the third chapter I contemplate rates of landscape change in the uplands of a first-order sandstone-underlain catchment. Though these projects are at different locations and focus on different aspects of landscape change, the uniting

question I ask is: how have changes in climate and base level influenced the development and transport of regolith in Pennsylvania?

1.2 Climate in the Pleistocene and periglaciation

One of the strongest drivers of millennial-scale landscape change in Pennsylvania has been climate, specifically glacial/interglacial cycles. The Laurentide ice sheet advanced into Pennsylvania at least four times in the Pleistocene, making areas proximal to, but not covered by, the glacier 'periglacial'. Periglaciation is a state in which which cold-based weathering processes control the formation and movement of regolith (Clark and Ciolkosz, 1988; French and Millar, 2014). Periglaciation is usually, but not always, accompanied by perennially frozen ground (Péwé, 1983).

The last global glacial maximum was ~30 ka (Lambeck et al., 2014), but the regional last glacial maximum was likely~26 ka, as defined by dating of the terminal moraine in New Jersey (Corbett et al., 2016a). The exact ages of all prior glaciations are poorly constrained. The penultimate glacial maximum boundary is thought to be "Illinoian", or 130 ka (Sevon, 2000), but this date was originally produced by correlation to type localities in the Midwestern United States, not by numerical dating. The oldest glacial deposits in the state are at a minimum of 770,000 years old, as they include glacial lake sediments with reversed magnetic polarity.

Cold conditions at past glacial maxima have left relict 'periglacial' landforms throughout the central Appalachians. These landforms cannot be formed in the modern climate regime and are created by strong frost action, intensive mass wasting, and eolian activity. These relict landform are suggestive of, but not diagnostic of periglacial activity,

2

and can include block streams, block fields, sorted ground, talus slopes, and solifluction lobes (Clark and Ciolkosz, 1988; Nelson et al., 2007; Péwé, 1983). Conventionally, periglaciation has been invoked as a force that 'wiped the slate clean' in the Appalachians by increasing erosion rates by an order of magnitude, decreasing relief by increasing erosion rates in the uplands (Braun, 1989).

1.3 Erosion and relief in the Appalachians

Orogeny in the Appalachian mountain chain ceased millions of years ago, yet the mountains remain. The persistence of relief in the Appalachians has been a long-standing debate in geomorphology. Willam Morris Davis's *Geographical Cycle* was inspired by his observations of the Appalachians, in which he proposed that given time, a mountainous landscape will erode until only a flat 'peneplain' exists (Davis, 1889). Many years later Hack (1960) proposed a different theory of landscape evolution, 'dynamic equilibrium'. Hack's theory was that the landscape wouldn't erode down to a peneplain, rather it would develop a 'steady state' in which slope adjusts to lithology to account for differences in rock strength. A landscape in dynamic equilibrium would have consistent rates of erosion across the landscape. Hack proposed that erosion rates would be independent of slope as well as lithology, but that more resistant rocks should form steeper slopes.

The debate over the nature of Appalachian landscape evolution continues today. Recently research has shown that the Appalachians are not eroding towards a peneplain, rather that relief has increased since the Miocene (Miller et al., 2013). The explanation for this increase in relief is not simple. Hancock and Kirwan (2007) suggest that this

relief is a signature of climate, and that rapid shifts in climate 3-4 m.y. ago may have led to a widespread acceleration of erosion rates (Mills, 2000). Workers have alternately argued for stream capture and drainage reorganization as the drivers of topography (Pazzaglia and Brandon, 1996; Prince and Spotila, 2013). Most recently this relief has been attributed to epiorogenic uplift caused by mantle dynamics (Miller et al., 2013) and subsidence-induced differential erosion caused by sinking of the subducted Farallon slab (Liu, 2014)

Whatever the reason, the Appalachian region is likely not in a state of 'dynamic equilibrium'. Measured erosion rates demonstrate that Appalachian ridgelines erode at a slower pace than the fluvial network, which is incising down and increasing relief (Portenga et al., 2013). This fluvial incision is propagating up through the landscape like a wave, in the form of a series of breaks in the longitudinal profile called 'knickpoints'(Miller et al., 2013). These 'knickpoints' are clustered from 300-600 m but are not systematically related to transitions from weak to resistant substrate, rather they represent a wave of incision propogating up through the drainage system since sometime between 3.5-15 Ma (Miller et al., 2013).

CHAPTER 2: A HALF-MILLION YEAR OLD FOSSIL LANDFORM IN CENTRAL PENNSYLVANIA

2.1 Abstract

During glacial periods, land areas outside ice margins are frozen but remain unglaciated. In these periglacial zones, ice and sediment move downslope creating distinctive landforms. Among these landforms are boulder fields, low-gradient, unvegetated expanses of bare fractured rock that range from tens to hundreds of meters long. Periglacial boulder fields are ubiquitous features throughout the world, yet few age constraints exist on these features. Here we use *in-situ* cosmogenic ^{10}Be and ^{26}Al to estimate age and infer process at Hickory Run, one of the largest boulder fields in North America. This field is a 550 m long by 150 m wide nearly flat expanse of sandstone and conglomeritic clasts and boulders, some of which are more than 10 m long.

We find that ^{10}Be concentrations (n=52) increase downfield and are spatially autocorrelated. Boulder lithology, size, and position relative to the main axis of the field do not correlate with ^{10}Be concentration. All boulders have at least 70 ka of exposure; none have last glacial maximum (LGM) exposure ages. The majority of boulder ages fall between 130 and 200 ka, consistent with marine isotope stage 6 mapped as the Illinoian glaciation in Pennsylvania. However, 14 boulders have 300 ka or more of exposure; the greatest exposure age is 600 ka. Measurement of samples from the top and bottom of a boulder and three clasts beneath it demonstrate that rocks in the field move over time and are not only the result of in-situ weathering. Measured ^{26}Al/^{10}Be ratios ($n = 23$) suggest that boulders have remained near the surface and have been buried for less time than they were exposed.

5

The new isotopic data demonstrate that Hickory Run, and likely many other similar boulder fields in eastern North America are ancient, multigenerational features that have persisted over many glacial-interglacial cycles. These findings add nuance to the conventional view of periglaciation as a force that 'wiped the slate clean' in the Appalachian Mountains—in upland areas with resistant lithologies, we show that the landscape was reworked, but not reset by repeated periglaciation.

2.1 Introduction

Cycles of glacial retreat and advance in the Pleistocene caused large swaths of unglaciated North America to undergo periglaciation, a climate state in which frost action, intensive mass wasting, and eolian activity were the dominant geomorphic processes (Clark and Ciolkosz, 1988). Periglacial modification of the Appalachian Mountain region produced features that cannot form or are not active in the modern climate regime, particularly blockfields, boulder streams, and talus slopes (Braun, 1989; Clark and Ciolkosz, 1988), all of which can be found in close proximity to each other but are distinguished by differences in morphology, slope, and gradient (Wilson et al., 2016).

Tens if not hundreds of unvegetated periglacial boulder fields and streams exist in the eastern United States (Nelson et al., 2007; Potter and Moss, 1968; Psilovikos and Van Houten, 1982; Smith, 1953). These features are found not only in North America—they have been documented throughout the world in areas that have been subjected to Pleistocene periglaciation including (but not limited to) Australia (Barrows et al., 2004), South Africa (Boelhouwers et al., 2002), the Falkland Islands (Wilson et al., 2008), Italy

(Firpo et al., 2006), Norway (Wilson et al., 2016), and South Korea (Seong and Kim, 2003).

Cosmogenic nuclides such as ^{10}Be, ^{26}Al, and ^{36}Cl are produced by cosmic ray bombardment predominately in the uppermost few meters of Earth's surface, and can be used to provide age control for boulder deposits. Nuclide concentrations can be interpreted as an apparent surface exposure age, the time it would take for the measured concentration of a nuclide to build up in a sample exposed at the surface (Lal, 1991); however, accurate dating requires that several methodological assumptions are valid (Gosse and Phillips, 2001; Nishiizumi et al., 1993; Nishiizumi et al., 1991). Ages are modeled assuming that the sampled rock surface was a 'blank slate', not inheriting any nuclides from previous periods of exposure (Bierman et al., 1999; Colgan et al., 2002). Accurate ages also require no erosion or cover of the sampled surface by ice, soil, or other rocks after exposure. Exposure ages calculated from single nuclides cannot detect periods of burial and thus have the potential to underestimate total near-surface residence times (Bierman et al., 1999).

The few cosmogenic measurements made so far on periglacial block fields suggest that some were emplaced or at least active at the last glacial maximum, while others have existed for hundreds of thousands of years. Analysis of ^{36}Cl in 18 Australian boulder stream samples reveals a cluster of samples around 21 +/- 0.5 ka, consistent with the last glacial maximum, while other samples have exposure ages from 60 to 480 ka (Barrows et al., 2004). In contrast, block streams in the Falkland Islands show no evidence of last glacial maximum (LGM) activity; samples have ^{10}Be exposure ages

from 42 to 730 ka. (Wilson et al., 2008). Korean block streams also have pre-LGM exposure ages between 38 and 65 ka (Seong and Kim, 2003).

If rock surfaces have experienced significant burial after exposure, such complex histories can be detected by measuring two isotopes with different half-lives in the same sample. Two-isotope dating most commonly employs ^{26}Al and ^{10}Be which are produced in quartz at a ratio around 7 (Argento et al., 2013; Balco and Rovey, 2008; Balco and Shuster, 2009; Corbett et al., 2016b; Nishiizumi et al., 2007). When a sample is shielded after exposure by glacial ice or by other boulders, this ratio decreases as the 0.71 m.y. half-life of ^{26}Al (Nishiizumi et al., 1991) is shorter than the 1.38 m.y. half-life of ^{10}Be (Chmeleff et al., 2009; Korschinek et al., 2010). If a sample is re-exposed, production of nuclides begins again and the ratio increases. When using ^{26}Al and ^{10}Be, only long periods of burial (typically > 150 ka) can be detected reliably (Beel et al., 2016; Bierman et al., 2015). Burial dating (using ^{26}Al and ^{10}Be) has been used to show that boulders in two relict periglacial block streams have simple exposure histories (Seong and Kim, 2003; Wilson et al., 2008) with no extended burial.

Here we report 56 measurements of ^{10}Be and 23 measurements of ^{26}Al in boulders and outcrops in and near the Hickory Run boulder field, east-central PA. We use these data to infer processes affecting the field, to show that the field has existed for at least 600,000 years, and thus to conclude that it and thus many other periglacial features are likely the product of multiple glacial-interglacial cycles.

2.3 Geologic and Physiographic Setting

Hickory Run boulder field is situated 2 km south of the late Wisconsinan (LGM) Laurentide Ice Sheet boundary (Sevon and Braun, 2000) in east-central Pennsylvania, USA, (Fig. 1) a temperate, forested, soil-mantled inland region of the Atlantic passive margin. The field sits on a low-relief upland surface underlain by gently folded, resistant Paleozoic sandstones and conglomerates that have been scoured by glacial advance and retreat at least several times during the Quaternary (Sevon, 2000). The region is riddled with glacial erratics and small ponds produced by glacial scour and deposition.

The field is an elongate, 550 by 150 m wide, nearly flat (1°) open expanse of boulders in that runs parallel to the axis of a small valley and fills its headwaters (Smith, 1953). Hickory Run is bounded on both sides by sandstone ridgelines with ~30 m relief (Fig. 2). Boulders in the field range from <1 to >10 m long and are a very well indurated, exceptionally hard grayish-red medium grained sandstone and conglomeratic sandstone from the Ducannon member of the Catskill formation (Sevon, 1975). Upslope boulders (NE) (Fig. 2) are generally more angular than those downslope (SW) (Wedo, 2013), which tend to be more rounded and are often underlain by small, rounded, polished clasts with a red weathering rind (Fig 2). There is a distinct sub-section of the field to the southeast, where there are massive boulders that are mostly 5+ meters in length, and which appear to be bedrock shattered along bedding planes (Fig. 2). The entire field is bounded by coniferous forest with very stony loam and silt loam soils (NRCS, 2014). The forest appears to be slowly encroaching into the field, filling in open interstices with organic material (Fig. 2).

9

At least three pre-LGM glaciations extended over Hickory Run in the Pleistocene, though the total number and actual ages of pre-LGM deposits in Pennsylvania are poorly constrained (Braun, 2004). There are no obvious glacial erratics in the boulder field, all boulders appear to be locally sourced. The last glaciation to override Hickory Run is thought to be Illinoian (MIS 6), though it is possible that it was actually pre-Illinoian B (MIS 12) (Braun, 2004). South of the boulder field, reversed magnetic polarity deposits near the maximum limit of glaciation indicate that the oldest, most extensive glaciation was in the early Pleistocene (likely MIS 22). There is a MIS 16 event mapped in between the "Illinoian" event and the MIS 22 event, distinguished by proglacial lake sediments of normal polarity (Braun, 2004).

2.4 Methods

We sampled both across and down the field in order to test for spatial trends in ^{10}Be concentration. We sampled in 8 slope-normal transects and collected individual boulder samples by removing the uppermost few centimeters of rock using a hammer and chisel. We collected a total of 52 boulder samples from in and around the field. Of these samples, 43 were from boulders in the field, 5 were from bedrock tors outcropping on a nearby ridgeline, and one was from the bottom of a boulder (HR10B) accompanied by 3 clasts underneath it (HR10C1, C2, and C3) (Fig. 3A). We photographed each sample site and recorded the dimensions, sample thickness, and lithology of each boulder. Sub-meter resolution sample coordinates were recorded with a Trimble ProXH GPS™ unit and Zephyr™ antenna, post-processing the points against 2 base stations.

We purified quartz at the University of Vermont (Kohl and Nishiizumi, 1992) and extracted ^{10}Be and ^{26}Al from the 250-850 μm fraction following the methods

of Corbett et al. (2016). We measured ^{10}Be /^{9}Be ratios at Lawrence Livermore National Laboratory normalizing them relative to ICN standard 07KNSTD3110 with an assumed value of 2.85×10^{-12} (Nishiizumi et al., 2007); we corrected our data using an average of n=10 process blanks ($1.35\pm0.77 \times 10^{-15}$) and processed 4 replicate samples to test the reproducibility of our data. We then selected a subset of upslope (n=10) and downslope (n=9) boulder samples for ^{26}Al/^{27}Al analysis at PRIME lab, ensuring the distribution of the subset did not have a significantly different mean or variance from the population of 52 ^{10}Be measurements (Student's t test, $p = 0.76$, Bartlett test for equal variance $p =0.27$). Exposure ages were calculated using the CRONUS-Earth online calculator (http://hess.ess.washington.edu/, wrapper script 2.2, main calculator 2.1, constants 2.2.1, see Balco et al. (2008)) based on the constant production rate model (Lal, 1991; Stone, 2000a) using the regional northeastern United States production rate calibration dataset (Balco et al., 2009).

2.5 Results

Samples we collected have a range of ^{10}Be concentrations spanning nearly an order of magnitude, 0.44 to 3.26 x 10^6 atoms g^{-1} (Fig. 4). ^{26}Al concentrations range from 3.00 to 1.93 x 10^7 atoms g^{-1} (n=23), and correlate well with ^{10}Be measurements (r^2=0.99). ^{26}Al/^{10}Be ratios range from 5.43 to 7.36 and when plotted on a two isotope diagram are consistent with surface exposure and/or steady erosion (Fig. 5). There is no significant correlation between ^{10}Be concentration and boulder lithology, size, or position relative to the periphery of the field. Although ^{10}Be concentrations on ridgeline tors and the

southeastern sub-field tend to have lower concentrations than the main body of the field, the difference is not statistically significant at a confidence level of 95%.

Boulders downslope appear more rounded, are smaller, and have better developed weathering rinds than those upslope, suggesting that boulder weathering, and thus near surface residence time, increases downslope. Our results support this inference; the strongest correlation we find is between downslope distance and ^{10}Be concentration (r^2=0.45, Fig. 6). This spatial trend in ^{10}Be is visible in the model semivariogram, which demonstrates that boulder ages within the main body of the field become increasingly different with distance separating boulders (see GSA Supplemental Data Repository).

^{10}Be concentrations can be interpreted as either minimum limiting boulder exposure ages or maximum boulder surface erosion rates. When interpreted as ages, assuming simple exposure histories, no burial, and no inheritance, Hickory Run boulders have 70 to nearly 600 ka of surface exposure (Fig. 7). If considered as steady state erosion rates, boulders are eroding between 1 to 9 m/Ma. Boulders upslope (n=10) include the two youngest boulders (both 73 ka, adjacent to each other) and have ^{10}Be concentrations equivalent to an average of 136± 43 ka of exposure whereas downslope boulders (n =11) have been exposed for at least 382± 38 ka. The bedrock tor samples, in comparison, have an average exposure age of 159 ± 57 ka, not significantly different from upslope boulder exposure ages (Student's *t* test, *p* = 0.27). When interpreted as erosion rates, the tors appear to be eroding at a maximum rate of 3-7 m/Ma.

Our measurements of boulder HR10 and the clasts below it are not consistent with simple exposure in place (Fig. 3). The measured ^{10}Be concentration in sample 10B (from the underside of the boulder) is 170% of what would be expected if the boulder had

12

received all of its exposure in place, facing up (see GSA Supplemental Data Repository for calculations). Clasts C1, C2, and C3 contain more than three times the amount ^{10}Be than they should if they had been continuously underneath the boulder; all three clasts have higher concentrations of ^{10}Be than the sample from the top of the boulder.

2.6 Discussion

Hickory Run is an ancient, dynamic feature that has been exposed since at least the Middle Pleistocene (~ 600 ka). Cosmogenic exposure ages indicate not only that the field unambiguously predates the last glacial maximum (LGM) at 26 ka but that it persisted through multiple glacial/interglacial cycles. The lack of LGM ages anywhere in the field suggests that fresh boulders were not generated by periglaciation during the last period of climate cooling.

Most boulder exposure ages are between 100 ka and 200 ka; yet, Hickory Run is mapped within the Illinoian margin and thus, if the mapping and dating of the Illinoian are correct, under glacial ice at MIS 6 (Fig. 1). The old boulder ages, absence of glacial erratics within the field, and the lack of age constraints on the Illinoian glaciation (Braun, 2004) suggest that the 'Illinoian' glaciation in this part of Pennsylvania is older than MIS 6. If the mapping were correct, then any overriding ice must have been cold-based and non-erosive, as the boulder field was preserved rather than eroded. The preservation of block streams under cold-based ice is possible, and was documented by Kleman and Borgström (1990) as a mechanism of block stream preservation in west-central Sweden. Although we know little about glacial erosivity in prior North American glacial advances, cold-based ice is not unprecedented. Cosmogenic measurements of bedrock in the central

13

United States (Colgan et al., 2002), and on top of peaks in New England (Bierman et al., 2015) suggest that portions of the Laurentide were cold-based.

Isotopic measurements of samples from the top and the bottom of boulder HR10 as well as clasts underlying the boulder demonstrate that the boulder has moved rather than weathering in situ. Sample HR10T, exposed at the surface today, has a measured ^{10}Be concentration of 1.62 x 10^6 atoms g^{-1}; however, sample HR10B (on the underside of the boulder, 0.39 m below HR10T) contains 1.43 x 10^6 atoms g^{-1}, a far higher concentration than predicted based on the decrease of nuclide production with depth (Fig.3). Clasts underlying the boulder have higher concentrations of ^{10}Be than both boulder samples (1.68, 1.76 and 1.75 x 10^6 atoms g^{-1}).

This disparity in concentration with depth can be resolved if the boulder flipped after initial exposure and was then deposited on top of the clasts now underlying it. A simple model best matches the depth/production rate relationship for ^{10}Be if the boulder were flipped and deposited ~200 ka (Fig. 3, methods detailed in Supplemental Data). The 200 ka age of flipping is consistent with the large number of Hickory Run boulder exposure ages between 100-200 ka (Fig 4), and with the transition to the penultimate glacial period (MIS stage 6e, Railsback et al. (2015)). High nuclide concentrations in clasts provide further evidence for boulder movement. Clasts HR10 C1, C2, and C3 must not have been buried under boulder HR10 for long, as their nuclide concentrations are comparable to those of nearby surface boulders. ^{26}Al/^{10}Be ratios in HR10 C1, C2, and C3 are indistinguishable from the production ratio suggesting little to no burial, and are similar to those measured on nearby surface boulders. The boulder and associated clast

14

samples offer powerful evidence that the material in the Hickory Run field has been mobile in the past.

Cosmogenic isotopic measurements provide no unique solution to the origin and history of today's boulders but considered along with field observations better constrain how and when the field developed. It is possible the consistent increase in [10]Be exposure age with distance downfield results because boulders are derived from the upslope outcrop and are transported downslope over time. Alternately, this increase in age with distance could be from a frost-driven scarp retreat, in which the edge of the source outcrop incrementally retreated upslope and leaving a mantle of angular blocks in its place, producing progressively younger boulders upfield and leaving older boulders farther downslope to weather and round increasingly over time (André et al., 2008; Joyce, 1950). Our measurements cannot constrain which, if either, of these mechanisms produced the boulders that now make up Hickory Run.

New cosmogenic data reported here show that low-slope landscapes in the Appalachian Mountains are long-lived despite repeated climate change and periglaciation throughout the Quaternary. Despite its proximity to the latest Pleistocene Laurentide moraine (2 km), Hickory Run shows no sign of boulder production at the LGM, and erosion rates on ridgeline tors remain low (3 to 7 m/Ma) consistent with quartzite erosion rates elsewhere in the Appalachians and much farther from the glacial margin (5.5 m/ma, Portenga et al. (2013)).

Periglaciation is often invoked as a force that 'wiped the slate clean' in the northern Appalachians, rapidly stripping colluvium from slopes and depositing it into valleys (Braun, 1989); yet, the stability and persistence Hickory Run boulder field

suggest this is not always the case. Though periglacial activity moved boulders at

Hickory Run, our measurements demonstrate that low-slope landscapes built on resistant

lithologies are resilient enough to withstand multiple extended periods of periglaciation.

We conclude that Hickory Run and presumably many other boulder fields in the

Appalachian Mountains are old, dynamic, multigenerational features that have been

repeatedly reworked by periglaciation.

2.7 References

André, M.-F., Hall, K., Bertran, P., and Arocena, J., 2008, Stone runs in the Falkland Islands: Periglacial or tropical?: Geomorphology, v. 95, no. 3, p. 524-543.

Argento, D. C., Reedy, R. C., and Stone, J. O., 2013, Modeling the Earth's cosmic radiation: Nuclear Instruments and Methods in Physics Research Section B: Beam Interactions with Materials and Atoms, v. 294, p. 464-469.

Balco, G., Briner, J., Finkel, R. C., Rayburn, J. A., Ridge, J. C., and Schaefer, J. M., 2009, Regional beryllium-10 production rate calibration for late-glacial northeastern North America: Quaternary Geochronology, v. 4, p. 93-107.

Balco, G., and Rovey, C. W., 2008, An Isochron Method for Cosmogenic-nuclide Dating of Buried Soils and Sediments: American Journal of Science, v. 308, p. 1083-1114.

Balco, G., and Shuster, D. L., 2009, ^{26}Al–^{10}Be–^{21}Ne burial dating: Earth and Planetary Science Letters, v. 286, p. 570-575.

Balco, G., Stone, J. O., Lifton, N. A., and Dunai, T. J., 2008, A complete and easily accessible means of calculating surface exposure ages or erosion rates from ^{10}Be and ^{26}Al measurements: Quaternary Geochronology, v. 3, p. 174-195.

Barrows, T. T., Stone, J. O., and Fifield, L. K., 2004, Exposure ages for Pleistocene periglacial deposits in Australia: Quaternary Science Reviews, v. 23, no. 5-6, p. 697-708.

Beel, C., Lifton, N., Briner, J., and Goehring, B., 2016, Quaternary evolution and ice sheet history of contrasting landscapes in Uummannaq and Sukkertoppen, western Greenland: Quaternary Science Reviews, v. 149, p. 248-258.

Bierman, P. R., Davis, P. T., Corbett, L. B., Lifton, N. A., and Finkel, R. C., 2015, Cold-based Laurentide ice covered New England's highest summits during the Last Glacial Maximum: Geology, v. 43, no. 12, p. 1059-1062.

Bierman, P. R., Marsella, K. A., Patterson, C., Davis, P. T., and Caffee, M., 1999, Mid-Pleistocene cosmogenic minimum-age limits for pre-Wisconsinan glacial surfaces in southwestern Minnesota and southern Baffin Island; a multiple nuclide approach: Geomorphology, v. 27, no. 1-2, p. 25-39.

Boelhouwers, J., Holness, S., Meiklejohn, I., and Sumner, P., 2002, Observations on a blockstream in the vicinity of Sani Pass, Lesotho Highlands, southern Africa: Permafrost and Periglacial Processes, v. 13, no. 4, p. 251-257.

Braun, D. D., 1989, Glacial and Periglacial Erosion of the Appalachians: Geomorphology, v. 2, p. 233-256.

-, 2004, The glaciation of Pennsylvania, USA: Developments in Quaternary Sciences, v. 2, p. 237-242.

Chmeleff, J., Blanckenburg, F. v., Kossert, K., and Jakob, D., 2009, Determination of the 10Be half-life by multicollector ICP-MS and liquid scintillation counting: Nuclear Instruments and Methods in Physics Research Section B: Beam Interactions with Materials and Atoms, v. 268, no. 2, p. 192-199.

Clark, G. M., and Ciolkosz, E. J., 1988, Periglacial geomorphology of the Appalachian Highlands and Interior Highlands south of the glacial border—a review: Geomorphology, v. 1, no. 3, p. 191-220.

Colgan, P. M., Bierman, P. R., Mickelson, D. M., and Caffee, M., 2002, Variation in glacial erosion near the southern margin of the Laurentide Ice Sheet, south-central Wisconsin, USA: Implications for cosmogenic dating of glacial terrains: Geological Society of America Bulletin, v. 114, no. 12, p. 1581-1591.

Corbett, L. B., Bierman, P. R., and Davis, P. T., 2016, Glacial history and landscape evolution of southern Cumberland Peninsula, Baffin Island, Canada, constrained by cosmogenic 10Be and 26Al: Geological Society of America Bulletin, p. B31402. 31401.

Firpo, M., Guglielmin, M., and Queirolo, C., 2006, Relict blockfields in the ligurian alps (Mount Beigua, Italy): Permafrost and Periglacial Processes, v. 17, no. 1, p. 71-78.

Gosse, J. C., and Phillips, F. M., 2001, Terrestrial in situ cosmogenic nuclides: theory and application: Quaternary Science Reviews, v. 20, no. 14, p. 1475-1560.

Joyce, J. R., 1950, Stone runs of the Falkland Islands: Geological Magazine, v. 87, no. 2, p. 105-115.

Kleman, J., and Borgström, I., 1990, The boulder fields of Mt. Fulufjället, west-central Sweden-Late Weichselian boulder blankets and interstadial periglacial phenomena: Geografiska Annaler. Series A. Physical Geography, p. 63-78.

Kohl, C. P., and Nishiizumi, K., 1992, Chemical isolation of quartz for measurement of *in-situ* -produced cosmogenic nuclides: Geochimica et Cosmochimica Acta, v. 56, p. 3583-3587.

Korschinek, G., Bergmaier, A., Faestermann, T., Gerstmann, U. C., Knie, K., Rugel, G., Wallner, A., Dillmann, I., Dollinger, G., Gostomski, C. L. v., Kossert, K., Maiti, M., Poutivtsev, M., and Remmert, A., 2010, A new value for the half-life of 10Be by Heavy-Ion Elastic Recoil Detection and liquid scintillation counting: Nuclear Instruments and Methods in Physics Research B, v. 268, p. 187-191.

Lal, D., 1991, Cosmic ray labeling of erosion surfaces; in situ nuclide production rates and erosion models: Earth and Planetary Science Letters, v. 104, no. 2-4, p. 424-439.

Nelson, K. J. P., Nelson, F. E., and Walegur, M. T., 2007, Periglacial Appalachia: palaeoclimatic significance of blockfield elevation gradients, eastern USA: Permafrost and Periglacial Processes, v. 18, no. 1, p. 61-73.

Nishiizumi, K., Imamura, M., Caffee, M. W., Southon, J. R., Finkel, R. C., and McAninch, J., 2007, Absolute calibration of 10Be AMS standards: Nuclear Inst. and Methods in Physics Research, B, v. 258, no. 2, p. 403-413.

Nishiizumi, K., Kohl, C. P., Arnold, J. R., Dorn, R., Klein, J., Fink, D., Middleton, R., and Lal, D., 1993, Role of in situ cosmogenic nuclides (super 10) Be and (super 26) Al in the study of diverse geomorphic processes: Earth Surface Processes and Landforms, v. 18, no. 5, p. 407-425.

Nishiizumi, K., Kohl, C. P., Arnold, J. R., Klein, J., Fink, D., and Middleton, R., 1991, Cosmic ray produced ^{10}Be and ^{26}Al in Antarctic rocks; exposure and erosion history: Earth and Planetary Science Letters, v. 104, no. 2-4, p. 440-454.

NRCS, 2014, Soil Survey Geographic database for Pennsylvania: Forth Worth, Texas, U.S. Department of Agriculture, Natural Resources Conservation Sevice.

Portenga, E. W., Bierman, P. R., Rizzo, D. M., and Rood, D. H., 2013, Low rates of bedrock outcrop erosion in the central Appalachian Mountains inferred from *In Situ* 10Be concentrations: Geological Society of America Bulletin, v. 125, no. 1-2, p. 201-215.

Potter, N., and Moss, J. H., 1968, Origin of the Blue Rocks block field and adjacent deposits, Berks County, Pennsylvania: Geological Society of America Bulletin, v. 79, no. 2, p. 255-262.

Psilovikos, A., and Van Houten, F., 1982, Ringing rocks barren block field, east-central Pennsylvania: Sedimentary Geology, v. 32, no. 3, p. 233-243.

Railsback, L. B., Gibbard, P. L., Head, M. J., Voarintsoa, N. R. G., and Toucanne, S., 2015, An optimized scheme of lettered marine isotope substages for the last 1.0 million years, and the climatostratigraphic nature of isotope stages and substages: Quaternary Science Reviews, v. 111, p. 94-106.

Seong, Y. B., and Kim, J. W., 2003, Application of In-situ Produced Cosmogenic 10Be and 26Al for Estimating Erosion Rate and Exposure Age of Tor and Block Stream Detritus: Case Study from Mt. Maneo, South Korea: Journal of Korean Geographical Society, v. 38, no. 3, p. 389-399.

Sevon, W. D., 1975, Geology and mineral resources of the Hickory Run and Blakeslee quadrangles, Carbon and Monroe Counties, Pennsylvania, Commonwealth of Pennsylvania, Department of Environmental Resources, Bureau of Topographic and Geologic Survey.

Sevon, W. D., 2000, Map 13: Physiographic Provinces of Pennsylvania: Commonwealth of Pennsylvania Department of Conservation and Natural Resources Bureau of Topographic and Geologic Survey.

Sevon, W. D., and Braun, D. D., 2000, Map 59: Glacial deposits of Pennsylvania, Pennsylvania Department of Conservation and Natural Resources Bureau of Topographic and Geologic Survey.

Smith, H. T. U., 1953, The Hickory Run boulder field, Carbon County, Pennsylvania: American Journal of Science, v. 251, p. 625-642.

Stone, J., 2000, Air pressure and cosmogenic isotope production: Journal of Geophysical Research, v. 105, no. b10, p. 23753-23759.

Wedo, A. M., 2013, Boulder orientation, shape, and age along a transect of the Hickory Run Boulder Field, Pennsylvania [Master of Science in Geography: University of Delaware.

Wilson, P., Bentley, M. J., Schnabel, C., Clark, R., and Xu, S., 2008, Stone run (block stream) formation in the Falkland Islands over several cold stages, deduced from cosmogenic isotope (10Be and 26Al) surface exposure dating: Journal of Quaternary Science, v. 23, no. 5, p. 461-473.

Wilson, P., Matthews, J. A., and Mourne, R. W., 2016, Relict Blockstreams at Insteheia, Valldalen-Tafjorden, Southern Norway: Their Nature and Schmidt Hammer Exposure Age: Permafrost and Periglacial Processes, v. 28, no. 1, p. 286-297.
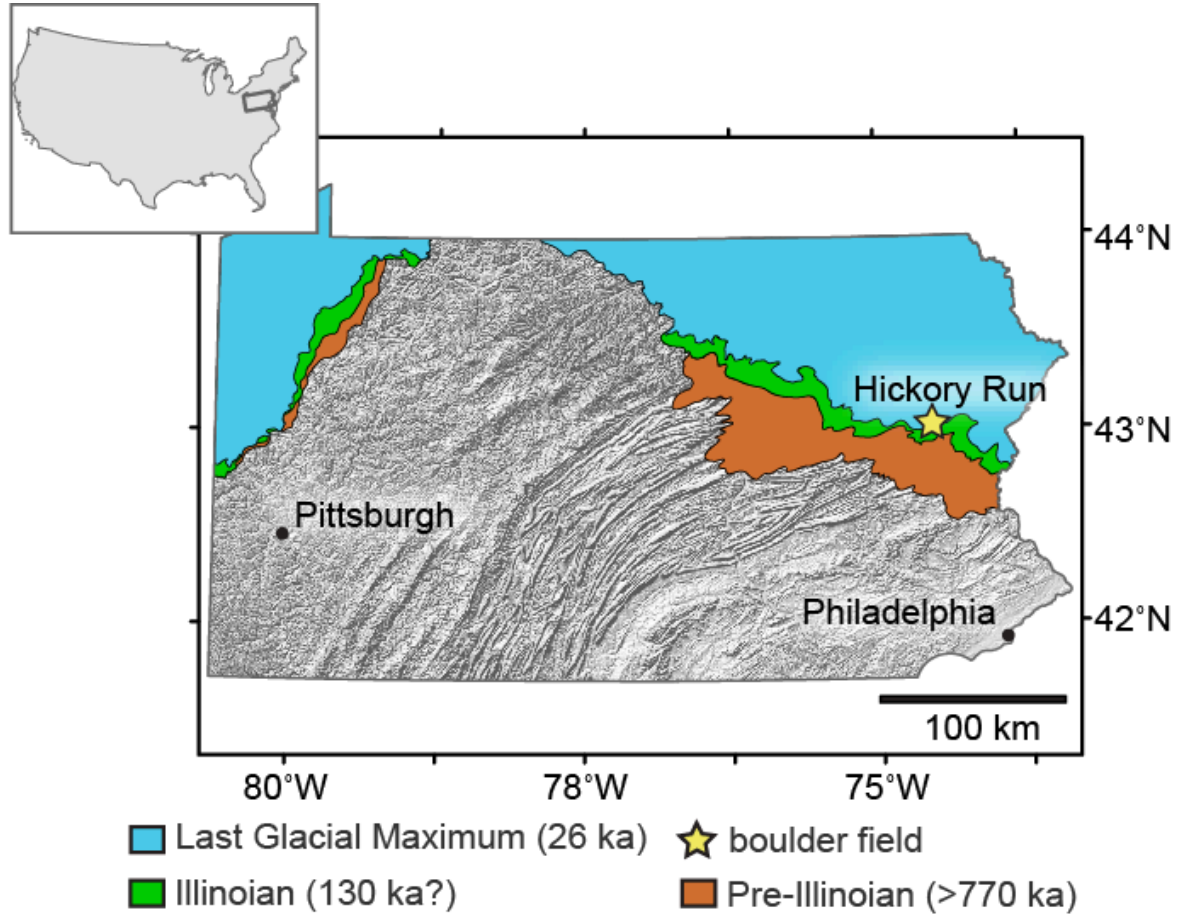
Figure 1. Location of Hickory Run in relation to the extent of the Last Glacial Maximum (26 ka), Illinoian (130 ka?), and pre-Illinoian glaciations, after Sevon and Braun (2000). Hickory Run is 2 km south of the LGM boundary and is mapped within the Illinoian and pre-Illinoian glaciations.
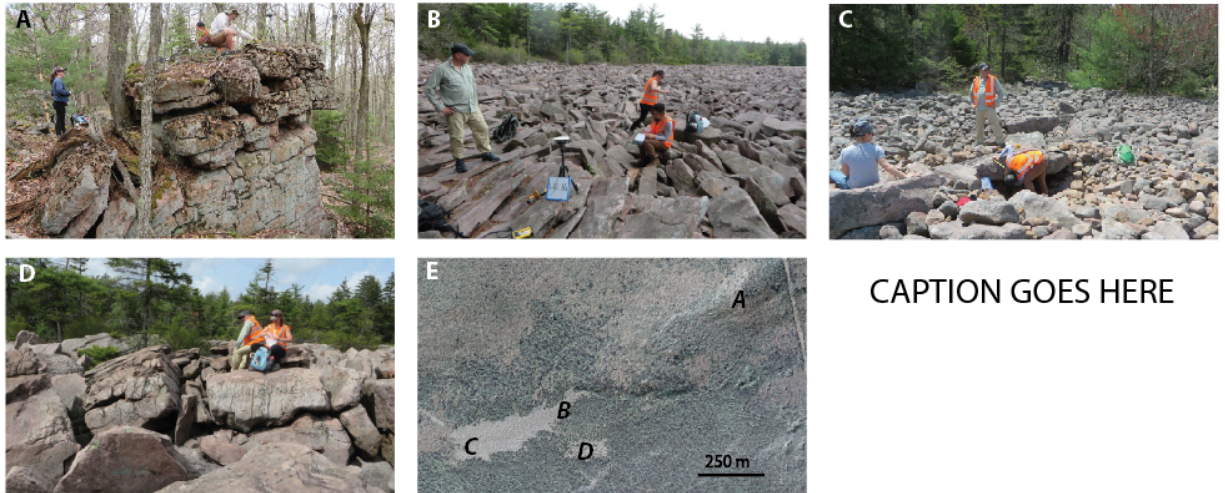
Figure 2. Photographs of field area including (A) the tors on a ridgeline northeast of the boulder field (B) elongate, larger boulders upslope in the main field (C) smaller, weathered boulders downslope, (D) massive conglomeritic boulders in the sub-field to the southeast of the main field, and (E) an aerial view of the Hickory Run Boulder field and surrounding forest.
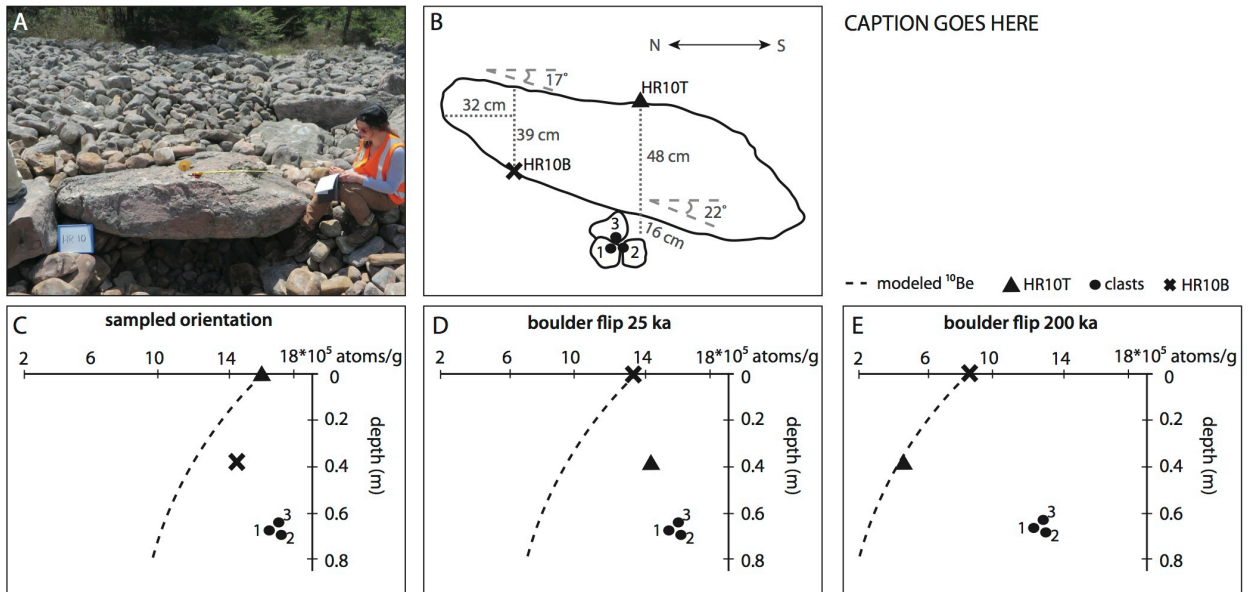
Figure 3: (A) Photograph of boulder HR10 on top of interlocked clasts, and (B) sketch of side view of HR10 and clasts. (C) ^{10}Be production decreases exponentially with depth. The black dotted line represents the ^{10}Be concentrations expected in HR10B and 10C1-C3 assuming they have remained in place at depth for their entire histories. (D) Depth profile assuming the boulder flipped 180° at 25 ka—the concentration in HR10T is too high to have flipped this recently. (D) Sample HR10T aligns with the depth profile assuming the boulder flipped at 200 ka.

21
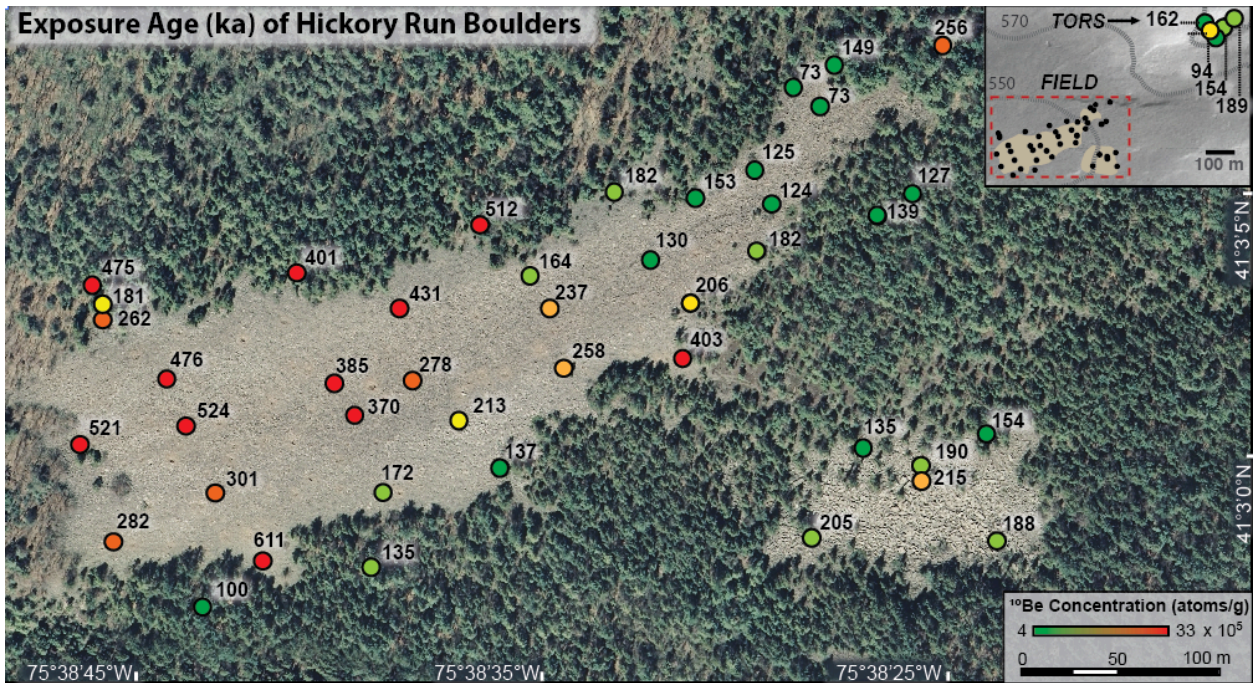
Figure 4: Exposure ages (ka) of Hickory Run boulders and tors. Inset shows location of tors relative to the main boulder field. Samples are color-coded by [10]Be concentration, red dots indicate higher [10]Be concentrations, green dots indicate lower [10]Be concentrations.
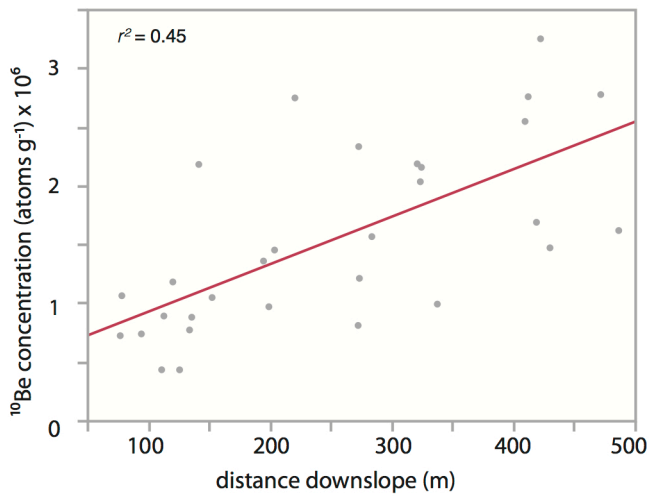
Figure 5. Positive correlation between [10]Be concentration and downslope distance in the main body of the field.
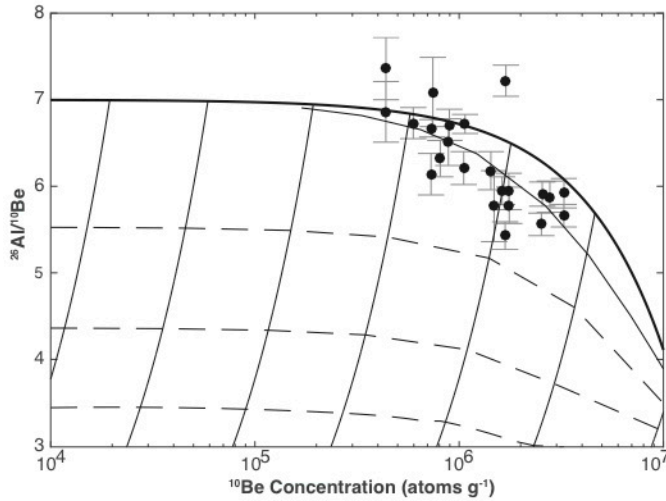
Figure 6: Measured ^{26}Al/^{10}Be ratios plotted against ^{10}Be concentrations ($n = 23$). Samples with simple exposure history (continuous exposure at the surface of the field with or without erosion) will plot within the banana-shaped envelope at the top of the plot. The thick black line indicates constant exposure at the surface, and the line beneath it marks the end of the 'erosion envelope'. Points plotting beneath this envelope have had at least one period of burial or shielding. Thin lines represent the trajectory that a sample would follow if buried, and dotted lines indicate burial isochrones of 0.5, 1.0, and 1.5 m.y. (top to bottom).

23
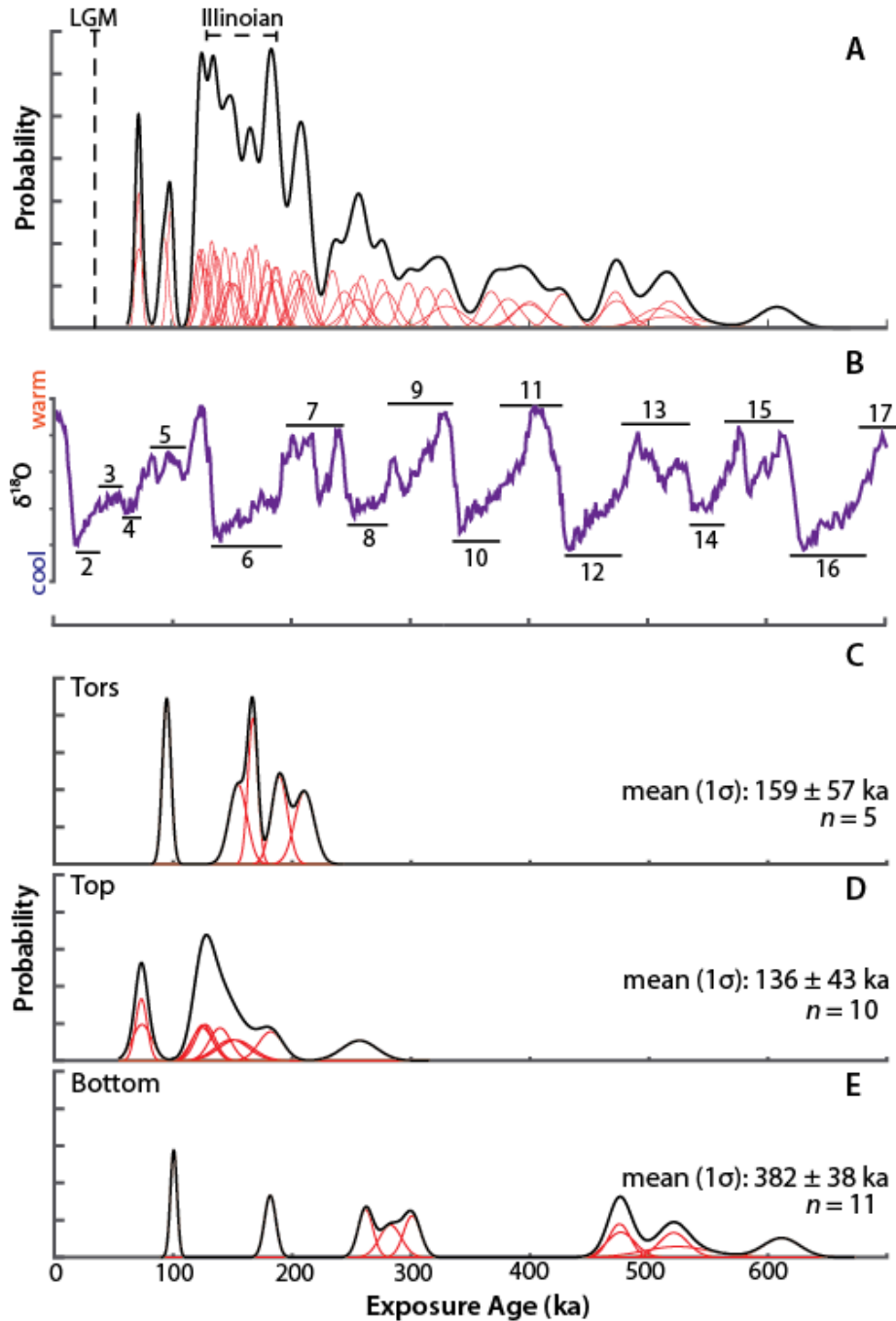
Figure 7: (A) Summed probability plot of all sample exposure ages plotted against (B) MIS curve of stable oxygen isotope ratios in deep sea foraminefera after (Railsback et al., 2015). Even numbers represent glacial stages, odd numbers are warmer interglacials. (C) Summed probability exposure ages of the tors, (D) of the 2 furthest downslope boulder transects (n=11), and (E) of the 3 boulder transects furthest upslope and surrounding forest samples. Each individual red curve represents a single [10]Be measurement and its 2σ internal error, the thick black line represents the sum of all samples.

24

Supplementary Materials

Contents:
1) Semivariogram and spatial autocorrelation of boulders
2) HR10 toppling and burial calculations

DR Figures:
1) Sample locations by name
2) Semivariogram
3) Box plots by boulder location and lithology

DR Tables:
1) Laboratory preparation and AMS analysis information
2) Sample location, boulder type, and CRONUS exposure age and erosion rate

1. Spatial Analysis

Semivariance is a spatial statistic that measures the dissimilarity between

measurements over a distance. Semivariance is defined by the equation:

$$\gamma(h) = \frac{1}{2N(h)} \sum_{i=1}^{N(h)} [u(a)_i - u(a+h)_i]^2 \qquad \text{(Eq. 1)}$$

Where $\gamma(h)$ is the semivariance, $N(h)$ is the total number of sample pairs separated

by a distance h, and $u(a)$ and $u(a+h)$ are the locations of a sample pair separated by h

(Isaaks and Srivastava, 1989; Portenga et al., 2013).

To create the semivariogram plot (A), I calculated the semivariance and distance

between every possible pair of ^{10}Be measurements from the main boulder field.

Semivariance is plotted on the y axis and lag distance (h) is plotted on the x axis. To

create the experimental semivariogram (B) I divided the semivariogram into 50 m bins

and plotted the average $\gamma(h)$ of each bin with 95% confidence interval. The third diagram

is the model semivariogram (C), in which an exponential model is fit through the points. The γ(h) value and the (*h*) value at which the model flattens out are called the 'sill' and 'range' respectively, and represent the point at which samples are no longer spatially autocorrelated. The model does not pass through the origin, it is projected to a point on the γ(h) axis >0. This discrepancy is caused by the inherent error in sample collection and measurement (Journel and Huijbregts, 1978).

The model semivariogram shown here has a sill of 1.25 x 10^{12}, a range of 450 m, and a nugget of .1 x 10^{12} (C). The range marks the point at which the consistent increase in $\gamma(h)$ ends. The model semivariogram demonstrates that boulders become increasingly different from each over the length of the field.

2. Boulder HR10 toppling and burial calculations

Cosmogenic nuclide production decreases exponentially with depth at Earth's surface according to the equation:

$$P(x) = P(0)e^{-(\rho x/\Lambda)}$$
(Eq. 2)

Where x is the depth (cm), ρ is the density (we assume 2.7 g/cm^3), Λ is the absorption mean free path for nuclear particles in the rock (with an assumed value of 160), and $P(0)$ is the production rate of the cosmogenic nuclide at the rock surface (Nishiizumi et al., 1991).

We sampled on the top (HR10T), bottom (HR10B), and clasts underneath (HR10C1-3) boulder HR10 in order to test whether [10]Be concentrations were consistent with continuous exposure in place. To do this, we solved Eq. 2 for the production rate at depth, assuming a surface production rate of 5.9 from the CRONUS exposure calculator using the northeastern United States production rate calibration dataset (Balco et al.,

2009), using version wrapper script 2.2, main calculator 2.1, constants 2.2.1,

(http://hess.ess.washington.edu/, see Balco et al. (2008)). We multiplied the percentage

of the surface production rate by the measured concentration in HR10T to calculate the

expected ^{10}Be concentration for each subsurface sample. The modeled concentrations

were an order of magnitude lower than the measured values, confirming that boulder

HR10 and the underlying clasts could not have been continuously oriented as they are

today.

After ruling out continuous exposure in place we created a simple model in which

the boulder flipped at 25 ka (the LGM). We subtracted 25 ka worth of ^{10}Be production

from each sample using the production rate at each respective depth and made a new

production curve, setting sample HR10B as the 'top' at 25 ka. Sample HR10 plots far to

the right of this curve and has too much ^{10}Be to have been exposed as recently as 25 ka.

When we repeat this exercise by subtracting 200 ka of exposure (the beginning of MIS 6,

the Illinoian glacial period) HR10B and HR10T align, consistent with a boulder flip at

200 ka. The clasts, on the other hand, have concentrations that are high on both curves,

suggesting that boulder HR10 has not always shielded the clasts.

**I will insert this portion on next interation.

Our third model was to test whether the ^{26}Al/^{10}Be would have been significantly

altered by 200 ka of burial under boulder HR10. Nuclides decay according to:

$$\frac{N_{26}}{N_{10}} = \left(\frac{N_{26}}{N_{10}}\right)_0 e^{-t_{burial}(1/\tau_{26}-1/\tau_{10})} \qquad \text{(Eq.3)}$$
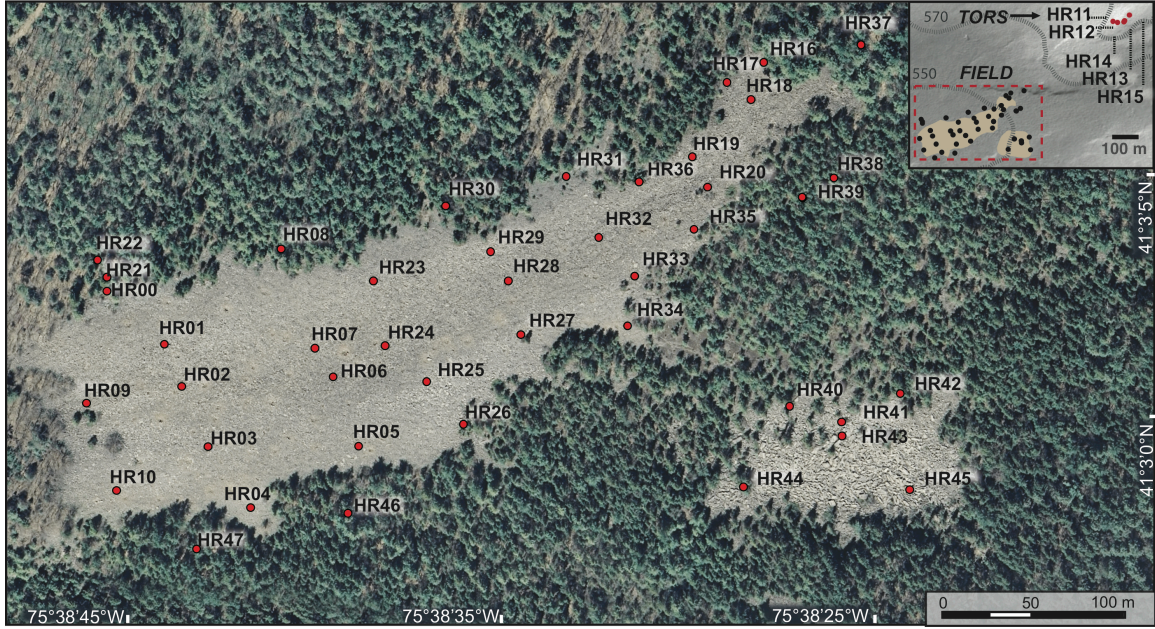
Figure DR1: Hickory Run sampling location map by name.
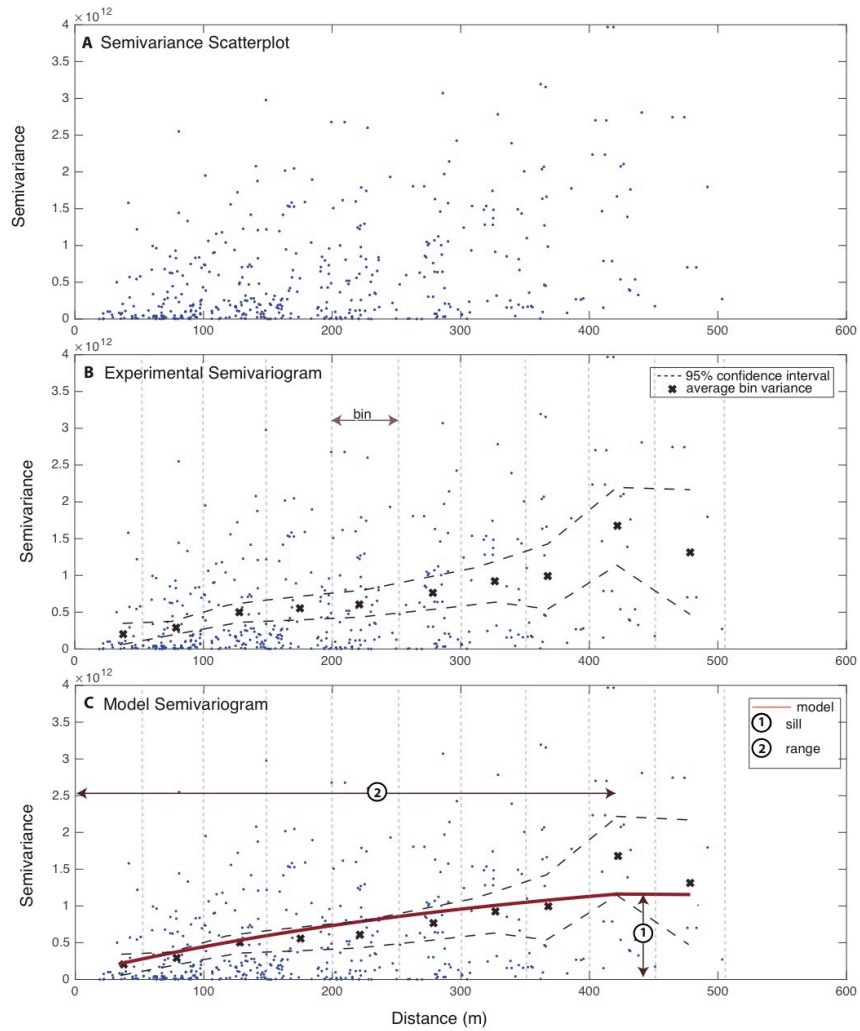
Figure DR2: Semivariogram of [10]Be measurements in boulders from the main field at Hickory Run. (A) Semivariance scatterplot, each point represents the calculated semivariance and distance between a boulder pair. Every permutation of two boulders from the main field is plotted. (B) Experimental semivariogram of the field, measurements are binned every 50 m and plotted with 95% confidence interval. (C) Model fit of the experimental semivariogram. Spatial autocorrelation ends between 400-500 m.
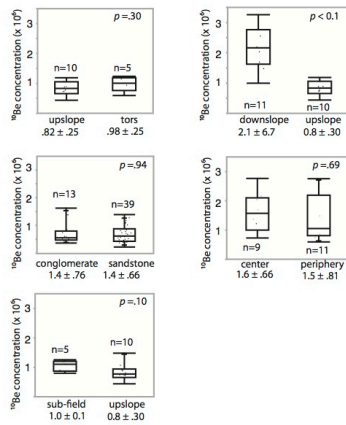
Figure DR3: Box and whiskers plots of boulder types, comparisons made using Student's *t*-test. The ends of the whiskers represent the range of 10Be concentrations, while the top, middle, and bottom of each box mark the 75th, 50th, and 25th percentiles.

Isaaks, E. H., and Srivastava, R. M., 1989, Applied geostatistics: Oxford University Press: New York, p. 561.

Journel, A. G., and Huijbregts, C. J., 1978, Mining geostatistics, Academic press.

Nishiizumi, K., Kohl, C. P., Arnold, J. R., Klein, J., Fink, D., and Middleton, R., 1991, Cosmic ray produced ^{10}Be and ^{26}Al in Antarctic rocks; exposure and erosion history: Earth and Planetary Science Letters, v. 104, no. 2-4, p. 440-454.

Portenga, E. W., Bierman, P. R., Rizzo, D. M., and Rood, D. H., 2013, Low rates of bedrock outcrop erosion in the central Appalachian Mountains inferred from *in situ* ^{10}Be concentrations: Geological Society of America Bulletin, v. 125, no. 1-2, p. 201-215.

CHAPTER 3. BEDROCK MATTERS: LITHOLOGIC CONTROL OF EROSION RATES OVERWHELMS EFFECT OF BASE LEVEL FALL

3.1 Abstract

Both base level and lithology influence erosion rates at a basin scale. Here, we exploit measurements of *in-situ* ^{10}Be in 17 fluvial sediment samples from Young Woman's Creek, a 230 km^2 unglaciated, headwaters drainage basin in central Pennsylvania. This watershed is in Appalachian Plateau physiographic province, a recently incised landscape on the Atlantic North American passive continental margin that is adjusting to changes in local base level that have occurred over the past several million years. We find that knickzones along channel profiles are predominantly distributed in the headwaters of the basin between 300 and 550 masl, and that 15 of the 17 identified knickzones have contributing drainage areas of <5 km^2. Of the 17 knickzones, 8 are associated with stepwise increases in drainage area or breaks in lithology. Erosion rates are positively correlated with slope, but correlate negatively with normalized channel steepness, k_{sn}, and downstream distance. Though the basin has remnants of a unincised, 'relict', upland landscape, erosion rates are often highest in areas of low k_{sn}, and appear largely controlled by variations in rock strength in the underlying sandstone formations. Our results demonstrate the effects of lithology and base level on erosion rate are difficult to disentangle, and that when studied on a small scale (1-200 km^2), lithology can exert strong control over the spatial variability of erosion even in a landscape still responding to baselevel fall.

2.2 Introduction

Differences in lithology and falls in base level of a landscape can both affect the rate and spatial distribution of incision and thus modulate erosion rates. Lithologic contrasts and waves of incision moving upstream can be similarly expressed on the landscape as 'knickzones', or breaks in the longitudinal stream profile (Cyr et al., 2014). At the regional scale (tens of thousands of km^2), changes in the base level dictate erosion rates independently of lithology (Miller et al., 2013), but on a smaller scale (<200 km^2) which matters more, lithology or base level control?

Fluvial incision can maintain relief in tectonically inactive settings long after orogeny has ceased (Miller et al., 2013). When a perturbation changes the elevation of a landscape in relation to its drainage point, a wave of incision propagates upstream as oversteepened deviations from the concave-up channel profile that separate the adjusted landscape downstream and the relict, not yet incised landscape upstream (Howard et al., 1994; Whipple and Tucker, 1999; Whipple and Tucker, 2002). Common base level-perturbing processes include dynamic uplift (Gallen et al., 2013; Miller et al., 2013), climate change (Boettcher and Milliken, 1994; Hancock and Kirwan, 2007), subsidence-induced differential erosion (Liu, 2014), and stream capture (Willett et al., 2014). Transient (migratory) knickzones dictate erosion rates at a basin scale and separate the actively adjusting channel with steeper slopes and higher erosion rates downstream from the slowly-eroding 'relict' landscape upstream. When a steady state landscape is perturbed by base level fall, knickzones migrate at a pace set by upstream drainage area, local channel slope, and erosional process and rock strength (Whipple and Tucker, 1999).

Knickzones can be identified through the analysis of longitudinal stream profiles. A stream in a steadily eroding landscape is adjusted to upstream area, erosion rate, and the amount of material it transports. The form of such a stream profile is described by the stream power model of incision, a series of equations relating slope and drainage area (Hack, 1957; Kirby and Whipple, 2012).

$$S = k_S A^{-\theta} \tag{1}$$

Where S represents local slope, A is the upstream drainage area (a proxy for discharge), and k_S is a steepness index, and θ is a concavity index. However, since small changes in θ cause large changes in the steepness index, a 'normalized steepness index', $k_{sn,}$ is calculated to account for the changes in profile gradient due to drainage area (Wobus et al., 2006a). To do this, a reference concavity index, θ_{ref} is calculated by finding the slope of the regression line between gradient and drainage area at any given point on the stream network on a log-log plot.

$$S = k_{sn} A - \theta_{ref} \tag{2}$$

In a landscape under 'steady state', where uplift of rock is balance by erosion, channels undergoing incision exhibit higher k_{sn} values (Wobus et al., 2006a). However, knickzones can also be formed when a river encounters a change in lithology, as a channel flowing over a more resistant rock type assumes a steeper form (Hack, 1957).

Longitudinal stream profile analysis can be paired with [10]Be-based estimates of basin scale erosion rates to determine whether erosion rates are governed by differences in bedrock erosivity or by a migrating wave of incision. [10]Be is produced by cosmic ray interaction with earth materials (Gosse and Phillips, 2001; Granger and Muzikar, 2001;

Lal, 1998), and when measured in stream sediments, reflects spatially averaged erosion rates upstream of the sample site (Bierman and Steig, 1996; Brown et al., 1995; Granger et al., 1996).

In this paper, we investigate the influence of base level and lithology on erosion rates in a region shown to be responding to a transient fall in base level (e.g., Miller et al., 2013). We combine longitudinal stream profile analyses paired with 17 measurements of *in-situ* produced [10]Be in fluvial sediments from Young Womans Creek, a sandstone-underlain catchment in the headwaters of the Appalachian Plateau. We find that erosion rates in Young Womans creek correlate negatively with k_{sn}, and our results demonstrate that the influence of transient fluvial incision on erosion rates as suggested by Miller et al. (2013) is scale-dependent. In low-order watersheds with small drainage areas, lithology exerts a much larger role in the propagation of a transient wave of incision through the watershed, and it thus is difficult to disentangle the control of lithology versus that of base level on millennial-scale erosion rates.

3.3 Study Area

Young Womans Creek is a ~230 km^2 forested tributary of the West Branch Susquehanna River in the temperate, forested, unglaciated portion of the Appalachian Plateau province in north central Pennsylvania. The Susquehanna Basin is in a state of disequilibrium where a fall base level has caused river incision to outpace hillslope lowering rates, increasing relief through the propagation of knickzones up the channel network (Hancock and Kirwan, 2007; Miller et al., 2013; Portenga et al., 2013). This

change in base level originated millions years ago, most likely due to dynamic topographic uplift (Miller et al., 2013) or from tilting of the continent in response to the subsidence of the Farallon slab (Liu, 2014). Evidence for such baselevel change nearby is a knickzone in Cooks Run, a 50 km^2 catchment 15 km upstream of Young Womans Creek (Miller et al. (2013). The measured erosion rate upstream of the Cook's Run knickzone is fairly low (16 m/My) in comparison to the regional sandstone erosion rate below knickzones (52 ± 15 m/My, Miller et al. (2013)).

Young Womans Creek is underlain by Upper Devonian and Missisippian sandstones that vary in rock strength, primarily the Catskill, Huntley Mountain, Burgoon, and Pottsville Formations. The Huntley Mountain formation is comprised of greenish-gray flaggy lithic sandstones and siltstones, whereas the Catskill, Burgoon, and Pottsville formation are more quartz-rich and are common ridge-forming lithologies in the Appalachians (Berg, 1979) and thus appear more resistant to erosion. The structure of Young Womans Creek is controlled NE-SW trending anticlines and synclines. The headwaters of the Left Branch Young Womans Creek (NW) are underlain by the Catskill and Huntley Mountain formations, and have higher drainage density than the Right Branch (NE), underlain by the Pottsville and Burgoon formations (Colton and Luft, 1965).

Hillslopes at the highest elevations in the basin are gently sloping (<5°), but rapidly transition downstream into areas of higher slope and greater relief. Stream channels are both bedrock and alluvial, though smaller tributaries near the mouth of the basin are characterized by steep, step-pool segments with small waterfalls exposing

bedrock beneath. Sand is abundant in the headwaters but is sparse downstream where gravel and ~30-100 cm wide tabular clasts dominate.

3.4 Methods

We used a National Elevation Dataset 1/3-arc-second digital elevation model (DEM, 1/3 arc-second resolution projected to Universal Transverse Mercator, cell size 10 m) and the Stream Profiler Tools code (available at http://geomorphtools.org/) to extract longitudinal profiles from all tributaries within the basin, to mark knickzones on log slope versus log area plots of tributaries (Fig. 1), and to generate a k_{sn} layer of the entire drainage network based on a θ_{ref} of 0.45. Extraction techniques and plots are based on Wobus et al. (2006b) and Whipple et al. (2007). We marked knickzones in drainage areas > 1 km^2, as smaller basins were not large enough for us to determine whether the spike in the log slope-area plot was actually representative of a true knickzone, or only representative of the transition from colluvial to fluvial transport.

We collected 17 fluvial sediment samples across a range of subbasin slopes representative of the distribution of slopes in the catchment. We chose sample sites on the mainstem of the Right and Left Branch as well as ~20 m above tributary junctions, sieving samples to the 250-850 μm sand fraction. We purified quartz from these samples (Kohl and Nishiizumi, 1992), and extracted ^{10}Be following the methods of Corbett et al. (2016c). ^{10}Be $/^9$Be ratios were measured at Lawrence Livermore National Laboratory in July 2017 normalizing them relative to ICN standard 07KNSTD3110 with an assumed value of 2.85×10^{-12} (Nishiizumi et al., 2007); we corrected our data using an average of n=3 process blanks ($6.43 \pm 2.00 \times 10^{-16}$). We calculated the average elevation of each

subbasin from the 1/3-arc-second digital elevation model and entered these values into the CRONUS online erosion rate calculator (http://hess.ess.washington.edu/; Balco et al. (2008)) wrapper script version 2.3, calculator 2.1, function 2, constants 2.3, muons 1 using default calibration dataset.

3.5 Results

^{10}Be concentrations in Young Womans Creek sediment range from 1.03 ± 0.02 to 4.03 ± 0.09 x 10^5 atoms g^{-1} (Table 1) and resulting erosion rates range from 10 to 42 m/My, with a mean of 23 ± 9 m/My (1σ) (Table 2). Erosion rates do not correlate with subbasin area (r^2=0.04, r^2 adj= -0.02), but increase linearly with slope ($r^2 = 0.50$, Fig. 2) and decrease linearly with mean basin k_{sn} ($r^2 = 0.25$) (Fig. 3). Average basin k_{sn} values are lowest in the headwaters and increase downstream, with high values in small tributaries normal to the trunk stream (Fig. 4).

The mean erosion rate of trunk streams (23 ± 3 m/My, n =7) is indistinguishable ($p = 0.57$) from the mean tributary stream erosion rate (21 ± 11 m/My, n =10, Fig. 5). Erosion rates are highest in samples YW09, YW10, and YW 11 (42 ± 1.1, 30 ± 1.0, and 34 ± 0.7 m/My), all collected from basins underlain by the Catskill and Burgoon formations (Fig. 4). The lowest erosion rates are in subbasins in the northeastern headwaters (YW12 and YW13, 13 ± 0.3 and 11 ± 0.2 m/My), as well as in the headwaters of small tributaries normal to the mainstem in the southwest of the basin (YW07 and YW17, 13 ± 0.3 and 10 ± 0.3 m/My), predominantly underlain by the Burgoon and Pottsville formations.

Knickzones span a range of elevations from 315 to 520 masl, and are frequently upstream of confluences in subbasins with drainage areas <5 km^2. Of the 17 knickzones identified, 15 had upstream drainage areas smaller than 10 km^2 (Fig. 4), 4 fell on the contact between the Huntley Mountain and Catskill Formation, and 5 were immediately below stream junctions where drainage area increases stepwise. The knickzones that are not associated with a stepwise increase in drainage area or with a lithologic contact (n=9) tend to be in headwater basins with low k_{sn} values (n=8).

The average distance from the beginning of a knickzone to the outlet of the basin is 21 ± 6 km, and the average distance from the headwaters is 4.2 ± 2.2 km; there is no correlation between the two, nor is there a correlation between basin area and knickzone distance from the outlet. Both quickly (>30 m/My) and slowly (<14 m/My) eroding headwater subbasins contain knickzones. Knickzones are absent from most trunk streams, except for one on Shingle Branch (the westernmost branch in Left Branch Young Womans Creek, Fig. 3). Knickzones are not disproportionately found on any particular lithology.

3.6 Discussion

The spatial pattern of knickzones in Young Womans Creek is suggestive of an ongoing, transient wave of incision, yet lithology exerts the strongest control on erosion rate. Erosion rates in the uppermost reaches of Young Womans Creek vary by up to 30 m/My, and sub-basins that contain the ridge-forming resistant Burgoon and Pottsville formations erode far more slowly than northwestern basins that contain greater proportions of the weaker Huntley Mountain formation. Despite this lithologic

38

dependence, a wave of incision is clearly moving through the landscape. The correlation between basin slope and erosion rate is consistent with this (Riebe et al., 2000), as the steepening of hillslopes can represent the headward migration of knickzones (Prince and Spotila, 2013), and as unperturbed landscapes typically develop toward a form where both steep and gentle slopes erode similarly (Hack, 1975). Transience (incision) can also be inferred in the plot of the longitudinal profiles (Fig. 6), which show an inflection from convex to concave where the 'relict' low-slope landscape transitions downstream to the 'new' adjusted fluvial network. The presence of a non-lithologically-controlled knickzone in nearby Cooks Run is also supportive of regional landscape transience in response to base-level fall (Miller et al., 2013).

Though Young Womans Creek and Cooks Run only 15 km away from one another and have similar basin morphology, knickzone distribution and lithology differs between the two basins. Young Womans Creek has multiple knickzones, mostly found in small drainage areas (<10 km^2), whereas Cooks Run has one only knickzone, found in the mainstem (10 to 50 ^{k}m^2). Catskill/Huntley-underlain terrain in the headwaters of Young Womans Creek is quickly eroding (~35m/My), yet similar terrain in Cooks Run erodes at only 16 m/My, consistent with low erosion rates in a not-yet-perturbed relict landscape. The propagation of knickzones further upstream in Young Womans Creek is likely drainage area dependent—Cooks Run is only 50 km^2 whereas subcatchments in Young Womans Creek have nearby double the area. The only knickzone expressed in a trunk stream in Young Womans Creek is above sample YW06 on Shingle Branch, which has a drainage area similar to Cooks Run.

As basins get smaller, the movement of a transient becomes less efficient, as knickzone retreat hits a critical drainage area above which migration slows (Castillo et al., 2013; Crosby and Whipple, 2006; Weissel and Seidl, 1998). At this point the total stream discharge in each catchment is not enough to transport all debris away and the channel becomes too sediment-mantled to efficiently move the knickzone upstream. Instead of following the bedrock stream model of incision, hillslope processes and local rock strength take control of erosion (Weissel and Seidl, 1997). This decoupling of hillslope and channel processes likely contributes to the observed negative correlation between erosion rate and average k_{sn} in this basin. The pulse of incision in Young Womans Creek has moved far enough upstream that the surrounding bedrock governs the erosion rate; this explains why both the highest and the lowest measured erosion rates are measured in headwater with knickzones.

3.7 Conclusion

Erosion rates are governed by both base level and lithology, but in Young Womans Creek lithology matters more. The regional transient wave of incision has propagated to the uppermost reaches of the watershed where hillslope processes take control and the stream power model of incision no longer applies. Erosion rates in Young Womans Creek headwater streams range from 10 to 42 m/My, and correlate with mean subbasin slope, but they are decoupled from normalized steepeness index and are largely dependent on the predominant lithology. Results from this study confirm that knickzones can be 'hung up' in small drainages where hillslope processes influence erosion rates more strongly than fluvial incision does. Erosion rates in small-scale transient landscapes

can be highest on at the transition from the relict to the adjusted landscape, but only

where the local bedrock facilitates erosion.

References

Balco, G., Stone, J. O., Lifton, N. A., and Dunai, T. J., 2008, A complete and easily accessible means of calculating surface exposure ages or erosion rates from [10]Be and [26]Al measurements: Quaternary Geochronology, v. 3, p. 174-195.

Berg, T. M., 1979, The Huntley Mountain Formation: Catskill-to-Burgoon transition in north-central Pennsylvania, Department of Environmental Resources, Bureau of Topographic and Geologic Survey, v. 83.

Bierman, P. R., and Steig, E., 1996, Estimating rates of denudation and sediment transport using cosmogenic isotope abundances in sediment: Earth Surface Processes and Landforms, v. 21, p. 125-139.

Boettcher, S. S., and Milliken, K. L., 1994, Mesozoic-Cenozoic unroofing of the southern Appalachian Basin: Apatite fission track evidence from Middle Pennsylvanian sandstones: The Journal of Geology, v. 102, no. 6, p. 655-668.

Brown, E. T., Stallard, R. F., Larsen, M. C., Raisbeck, G. M., and Yiou, F., 1995, Denudation rates determined from the accumulation of in situ-produced 10Be in the luquillo experimental forest, Puerto Rico: Earth and Planetary Science Letters, v. 129, p. 193-202.

Castillo, M., Bishop, P., and Jansen, J. D., 2013, Knickpoint retreat and transient bedrock channel morphology triggered by base-level fall in small bedrock river catchments: The case of the Isle of Jura, Scotland: Geomorphology, v. 180, p. 1-9.

Colton, G. W., and Luft, S. J., 1965, Bedrock Geology of the Slate Run Quadrangle, Clinton, Lycoming, and Potter Counties, Pennsylvania, Commonwealth of Pennsylvania, Department of Internal Affairs, Bureau of Topographic and Geological Survey.

Corbett, L. B., Bierman, P. R., and Rood, D. H., 2016, An approach for optimizing in situ cosmogenic 10 Be sample preparation: Quaternary Geochronology, v. 33, p. 24-34.

Crosby, B. T., and Whipple, K. X., 2006, Knickpoint initiation and distribution within fluvial networks: 236 waterfalls in the Waipaoa River, North Island, New Zealand: Geomorphology, v. 82, no. 1-2, p. 16-38.

Cyr, A. J., Granger, D. E., Olivetti, V., and Molin, P., 2014, Distinguishing between tectonic and lithologic controls on bedrock channel longitudinal profiles using cosmogenic 10Be erosion rates and channel steepness index: Geomorphology, v. 209, p. 27-38.

Gallen, S. F., Wegmann, K. W., and Bohnenstiehl, D., 2013, Miocene rejuvenation of topographic relief in the southern Appalachians: GSA Today, v. 23, no. 2, p. 4-10.

Gosse, J. C., and Phillips, F. M., 2001, Terrestrial in situ cosmogenic nuclides: theory and application: Quaternary Science Reviews, v. 20, no. 14, p. 1475-1560.

Granger, D. E., Kirchner, J. W., and Finkel, R., 1996, Spatially averaged long-term erosion rates measured from in situ-produced cosmogenic nuclides in alluvial sediments: Journal of Geology, v. 104, no. 3, p. 249-257.

Granger, D. E., and Muzikar, P. F., 2001, Dating sediment burial with in situ-produced cosmogenic nuclides; theory, techniques, and limitations: Earth and Planetary Science Letters, v. 188, no. 1-2, p. 269-281.

Hack, J. T., 1957, Studies of longitudinal stream profiles in Virginia and Maryland, US Government Printing Office.

Hack, J. T., 1975, Dynamic equilibrium and landscape evolution, *in* Melhorn, W. N., and Flemal, R. C., eds., Theories of landform development: Binghamton, N.Y., SUNY Binghamton,, p. 87-102.

Hancock, G., and Kirwan, M., 2007, Summit erosion rates deduced from 10Be: Implications for relief production in the central Appalachians: Geology, v. 35, no. 1, p. 89-92.

Howard, A. D., Dietrich, W. E., and Seidl, M. A., 1994, Modeling fluvial erosion on regional to continental scales: Journal of Geophysical Research, B, Solid Earth and Planets, v. 99, no. 7, p. 13,971-913,986.

Kirby, E., and Whipple, K. X., 2012, Expression of active tectonics in erosional landscapes: Journal of Structural Geology, v. 44, p. 54-75.

Kohl, C. P., and Nishiizumi, K., 1992, Chemical isolation of quartz for measurement of *in-situ* -produced cosmogenic nuclides: Geochimica et Cosmochimica Acta, v. 56, p. 3583-3587.

Lal, D., 1998, Cosmic ray produced isotopes in terrestrial systems, *in* Goswami, J. N., and Krishnaswami, S., eds., Isotopes in the solar system; proceedings Proceedings of the Indian Academy of Sciences, Indian Academy of Sciences, Bangalore, India, p. Earth and Planetary Sciences 107, no. 104 (199812) 199241-199249.

Liu, L., 2014, Rejuvenation of Appalachian topography caused by subsidence-induced differential erosion: Nature Geosci, v. 7, no. 7, p. 518-523.

Miller, S. R., Sak, P. B., Kirby, E., and Bierman, P. R., 2013, Neogene rejuvenation of central Appalachian topography: Evidence for differential rock uplift from stream profiles and erosion rates: Earth and Planetary Science Letters, v. 369, p. 1-12.

Nishiizumi, K., Imamura, M., Caffee, M. W., Southon, J. R., Finkel, R. C., and McAninch, J., 2007, Absolute calibration of [10]Be AMS standards: Nuclear Inst. and Methods in Physics Research, B, v. 258, no. 2, p. 403-413.

Portenga, E. W., Bierman, P. R., Rizzo, D. M., and Rood, D. H., 2013, Low rates of bedrock outcrop erosion in the central Appalachian Mountains inferred from *in situ* [10]Be concentrations: Geological Society of America Bulletin, v. 125, no. 1-2, p. 201-215.

Prince, P. S., and Spotila, J. A., 2013, Evidence of transient topographic disequilibrium in a landward passive margin river system: knickpoints and paleo‐landscapes of the New River basin, southern Appalachians: Earth Surface Processes and Landforms, v. 38, no. 14, p. 1685-1699.

Riebe, C. S., Kirchner, J. W., Granger, D. E., and Finkel, R. C., 2000, Erosional equilibrium and disequilibrium in the Sierra Nevada, inferred from cosmogenic [26]Al and [10]Be in alluvial sediment: Geology, v. 28, no. 9, p. 803-806.

Weissel, J. K., and Seidl, M. A., 1997, Influence of rock strength properties on escarpment retreat across passive continental margins: Geology (Boulder), v. 25, no. 7, p. 631-634.

Weissel, J. K., and Seidl, M. A., 1998, Inland propagation of erosional escarpments and river profile evolution across the southeast Australian passive continental margin: Geophysical Monograph, v. 107, p. 189-206.

Whipple, K., Wobus, C., Crosby, B., Kirby, E., and Sheehan, D., 2007, New tools for quantitative geomorphology: extraction and interpretation of stream profiles from digital topographic data: GSA Short Course, v. 506.

Whipple, K. X., and Tucker, G. E., 1999, Dynamics of the stream‐power river incision model: Implications for height limits of mountain ranges, landscape response timescales, and research needs: Journal of Geophysical Research: Solid Earth, v. 104, no. B8, p. 17661-17674.

Whipple, K. X., and Tucker, G. E., 2002, Implications of sediment-flux-dependent river incision models for landscape evolution: Journal of Geophysical Research, B, Solid Earth and Planets, v. 107, no. 2.

Willett, S. D., McCoy, S. W., Perron, J. T., Goren, L., and Chen, C.-Y., 2014, Dynamic reorganization of river basins: Science, v. 343, no. 6175, p. 1248765.

Wobus, C., Whipple, K. X., Kirby, E., Snyder, N., Johnson, J., Spyropolou, K., Crosby, B., and Sheehan, D., 2006a, Tectonics from topography: Procedures, promise and pitfalls: Tectonics, climate, and landscape evolution: Geological Society of America Special Paper, v. 398, p. 55–74.

Wobus, C. W., Crosby, B. T., and Whipple, K. X., 2006b, Hanging valleys in fluvial systems: Controls on occurrence and implications for landscape evolution: Journal of Geophysical Research: Earth Surface, v. 111, no. F2, p. n/a-n/a.

Figures

Table 1. Laboratory preparation and AMS information.

Table 1. Laboratory Preparation and AMS Analysis Information

Sample	Quartz Mass (g)	^{9}Be Added (µg)	Be Cathode Number[1]	Measured ^{10}Be/^{9}Be[2]		^{10}Be/^{9}Be Uncertainty	^{10}Be concentration (atoms/g)		
YW01	21.546	248.11	BE40780	3.22E-13	±	6.00E-15	2.48E+05	±	4.62E+03
YW02	22.889	247.87	BE40781	2.39E-13	±	7.47E-15	1.73E+05	±	5.41E+03
YW03	20.557	247.31	BE40782	2.47E-13	±	7.67E-15	1.98E+05	±	6.17E+03
YW04	22.102	248.11	BE40783	2.88E-13	±	5.57E-15	2.16E+05	±	4.18E+03
YW05	24.659	247.31	BE40785	2.27E-13	±	4.40E-15	1.52E+05	±	2.95E+03
YW06	15.725	247.84	BE40786	1.42E-13	±	3.91E-15	1.50E+05	±	4.12E+03
YW07	22.255	246.78	BE40787	4.00E-13	±	7.74E-15	2.97E+05	±	5.73E+03
YW08	17.547	247.99	BE40817	1.34E-13	±	2.53E-15	1.27E+05	±	2.39E+03
YW09	18.027	247.34	BE40818	1.12E-13	±	2.82E-15	1.03E+05	±	2.59E+03
YW10	14.233	247.64	BE40819	1.23E-13	±	3.91E-15	1.43E+05	±	4.54E+03
YW11	20.146	247.70	BE40820	1.59E-13	±	3.75E-15	1.31E+05	±	3.08E+03
YW12	22.390	247.40	BE40788	4.36E-13	±	1.03E-14	3.22E+05	±	7.63E+03
YW13	22.034	246.84	BE40790	5.16E-13	±	9.58E-15	3.86E+05	±	7.18E+03
YW14	20.833	245.78	BE40791	1.95E-13	±	3.65E-15	1.54E+05	±	2.87E+03
YW15	20.366	246.90	BE40821	2.33E-13	±	5.42E-15	1.89E+05	±	4.39E+03
YW16	20.038	246.52	BE40814	2.44E-13	±	4.58E-15	2.00E+05	±	3.77E+03
YW17	20.301	247.17	BE40823	4.95E-13	±	1.19E-14	4.03E+05	±	9.65E+03

1. Identification for each sample within the database at the Center for Mass Spectrometry at Lawrence Livermore National Laboratory, Livermore CA.

2. Normalized using ICN standard 07KNSTD3110 with a ratio of 2.85 x 10-12 (Nishiizumi et al., 2007). Reported errors are 1σ AMS measurement uncertainties. Analyzed April 2016 using an average of n=3 process blanks ($6.43 \pm 2.00 \times 10^{-16}$).

Table 2. Sample location, concentration, and erosion rate.

Table 2. Sample location, concentration, and erosion rate

Sample	Latitude	Longitude	Elevation (m)	Erosion Rate (m/My)			Area (km²)	Mean Subbasin Slope (°)	Mean Subbasin K_{sn}	trunk or tributary
YW01	41.378	-77.706	486	16	±	0.3	1.3	11	885	tributary
YW02	41.374	-77.700	523	24	±	0.8	92.8	15	275	trunk
YW03	41.373	-77.697	552	21	±	0.7	123.9	14	336	trunk
YW04	41.393	-77.709	503	19	±	0.4	2.1	13	500	tributary
YW05	41.401	-77.707	529	27	±	0.6	28.5	15	245	trunk
YW06	41.401	-77.707	536	28	±	0.8	49.8	16	223	trunk
YW07	41.380	-77.718	514	13	±	0.3	0.7	5	--*	tributary
YW08	41.439	-77.703	547	34	±	0.7	41.9	16	203	tributary
YW09	41.464	-77.714	538	42	±	1.1	14.9	14	149	tributary
YW10	41.482	-77.682	566	30	±	1.0	12.7	13	144	tributary
YW11	41.505	-77.647	584	34	±	0.8	13.1	11	127	tributary
YW12	41.495	-77.607	608	13	±	0.3	14.3	7	248	tributary
YW13	41.470	-77.615	585	11	±	0.2	3.7	10	347	tributary
YW14	41.358	-77.705	537	27	±	0.5	220.1	14	314	trunk
YW15	41.450	-77.644	580	23	±	0.6	74.4	12	269	trunk
YW16	41.435	-77.663	574	21	±	0.4	92.9	13	289	trunk
YW17	41.402	-77.724	541	10	±	0.3	1.2	5	256	tributary

1. Erosion rates calculated using CRONUS calculator wrapper script version 2.3, calc. 2.1, function 2, constants 2.3, muons 1, default calibration dataset.

*drainage area too small for automated channel extraction
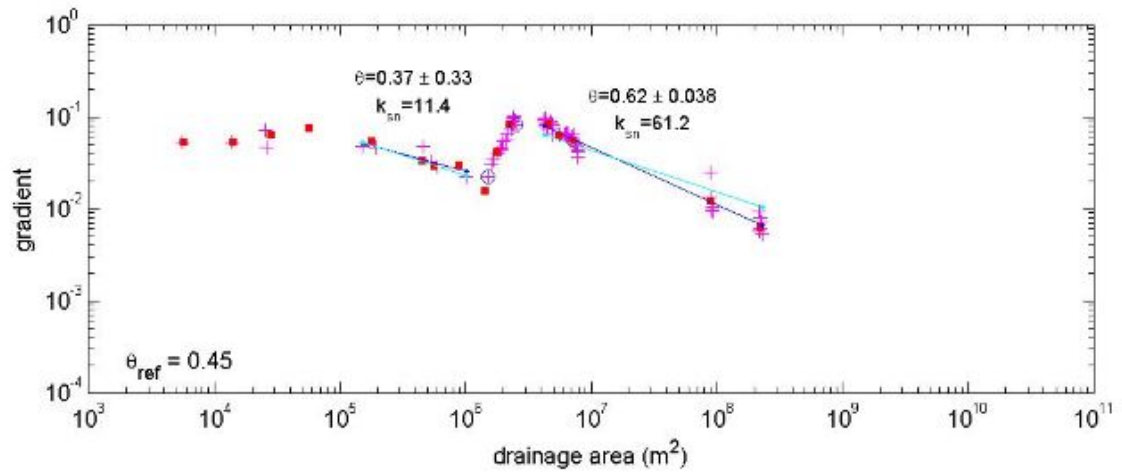
Figure 1. Example of a log slope-area plot used to identify knickzones. A knickzones is the break in between the linear fit upstream with low k_{sn} (11.4 in this image) and the linear fit downstream with high k_{sn} (61.2).
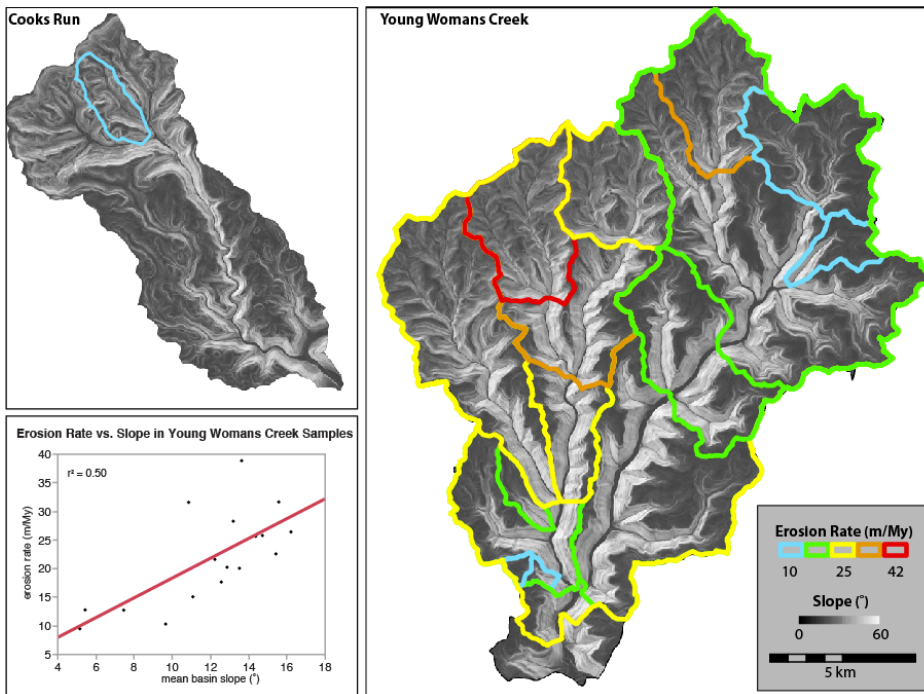
Figure 2. Slope and erosion rate in Cooks Run and Young Womans Creek watersheds. Slope correlates positively with erosion rate (r^2=0.50) in Young Womans Creek subbasins.

46
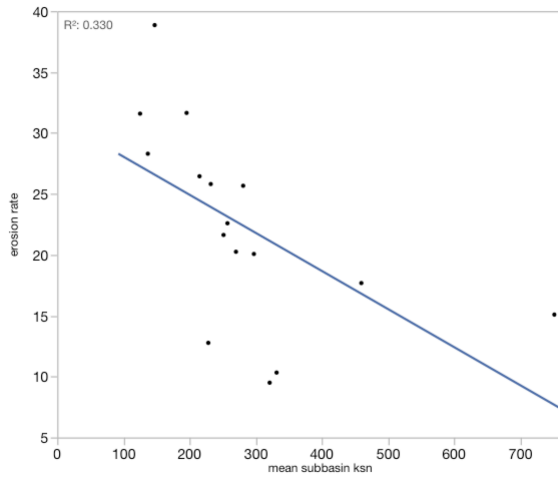
Figure 3. Normalized channel steepness (k_{sn}) correlates negatively with mean basin erosion rate.
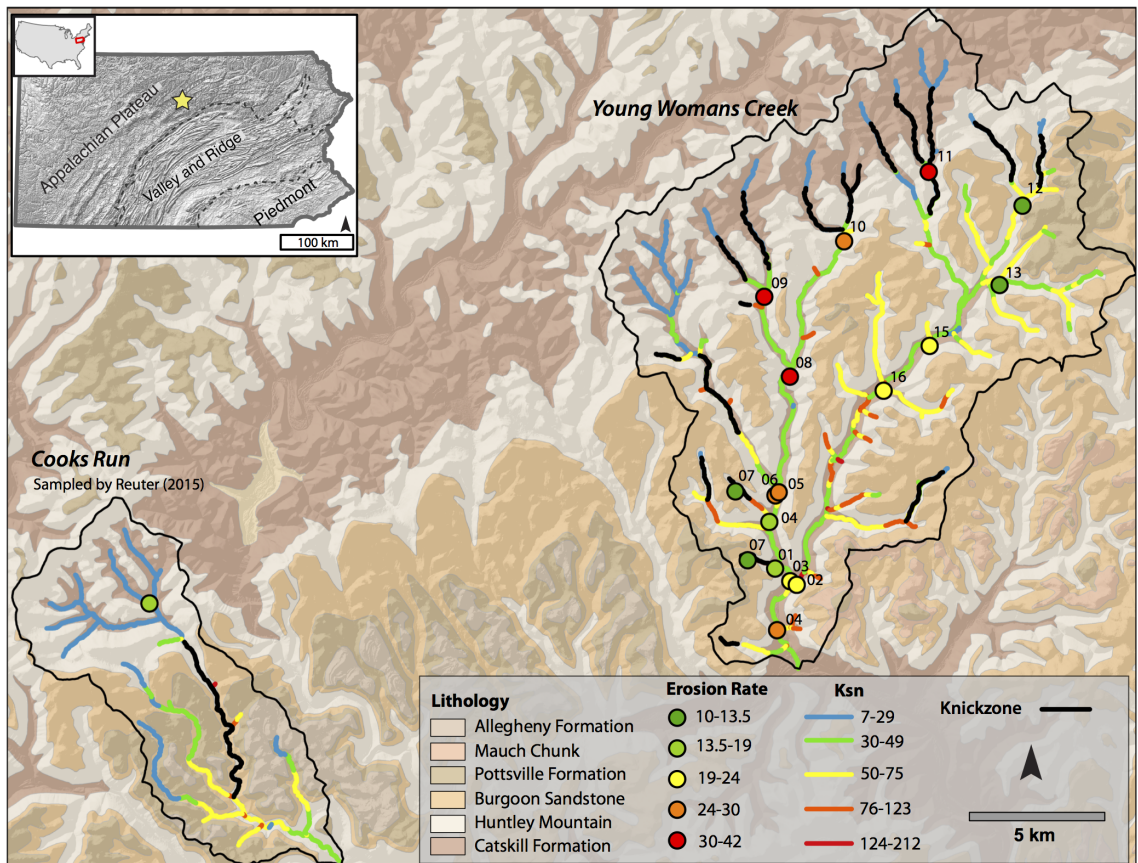
Figure 4. Study site location, lithology, sample locations, erosion rates, and k_{sn} in Young Womans Creek and Cooks Run watersheds. Cooks Run sample collection and processing was done by Reuter (2005).
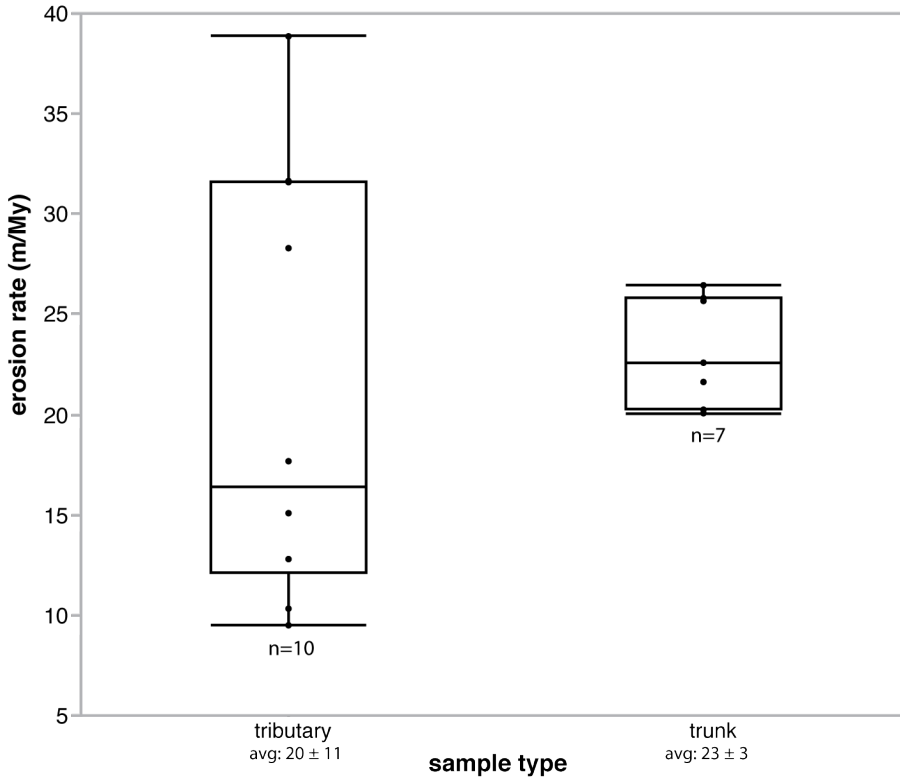
Figure 5. Erosion rates in tributaries vs. trunk streams. Trunk stream erosion rates vary less than tributary erosion rates, and are representative of the average erosion rate from the areas above.
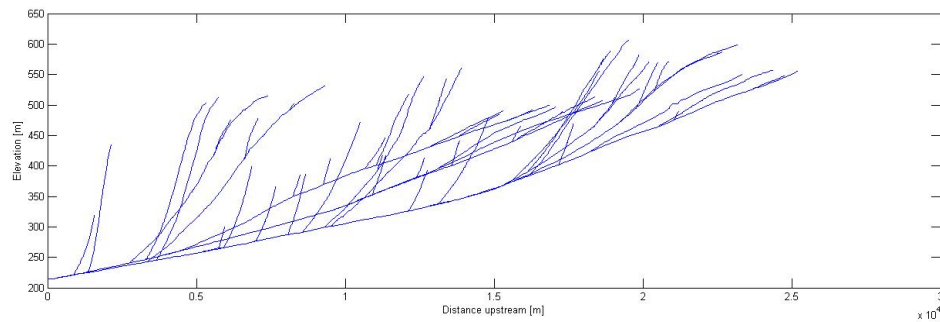
Figure 6. Transience (incision) can be inferred in the plot of the longitudinal profiles of all streams in Young Womans Creek, which show an inflection from convex to concave where the 'relict' low-slope landscape transitions downstream to the 'new' adjusted fluvial network

CHAPTER 4. GARNER RUN

4.1 Motivation

The Appalachian mountains persist in spite of the cessation of mountain building millions years ago (Baldwin et al., 2003), the exact reasons for which have been, and continue to be, a source of geomorphological debate (Gallen et al., 2013; Liu, 2014; Miller et al., 2013). The original model of landscape evolution was that of Davis (1899), who believed that the mountains were steadily eroding towards a flat peneplain, whereas Hack (1960) posited 'dynamic equilibrium', that the landscape would ultimately develop a 'steady-state' in which slope adjusts to lithology and the landscape erodes at a uniform rate. Today, it is recognized that the Appalachians are not in equilibrium, and that relief has increased since the Miocene (Gallen et al., 2013; Miller et al., 2013). Proposed explanations for this increase in relief have included climate change (Boettcher and Milliken, 1994; Hancock and Kirwan, 2007) and reorganization of the drainage network (Pazzaglia et al., 2006; Prince and Spotila, 2013), though most recently post-orogenic regional uplift (Gallen et al., 2013; Miller et al., 2013) and mantle-induced dynamic subsidence (Liu, 2014) have been the favored explanations. Rates of landscape change in the Appalachians are largely driven by this disequilibrium (Miller et al., 2013; Pazzaglia and Gardner, 1993), as well as by strong glacial/interglacial cycles (Braun, 1989). This chapter addresses Appalachian landscape evolution on a small scale, in which I use *in-*

situ [10]Be and [26]Al to constrain rates of landscape change in the headwaters of a small first-order Appalachian catchment in central Pennsylvania.

My work is supported by the Susquehanna Shale Hills Critical Zone Observatory (SSHCZO), an organization of scientists who investigate the 'critical zone', the area spanning the bedrock/regolith interface to the top of the tree canopy (Brantley et al., 2007). An understanding of the natural timescales over which surficial materials are formed and eroded away is fundamental to the study of soils, landforms, and the cycling of life-sustaining nutrients through the critical zone (Brantley et al., 2007). The SSHCZO was originally based in the Shale Hills catchment, a 0.8 km^2 first-order drainage in the Shavers Creek watershed, central PA. The observatory has since expanded to include Garner Run, a 1 km^2 study site in the headwaters of a sandstone-underlain drainage basin also within the Shavers Creek watershed. By comparing these two sites, which are 3 km apart and have experienced similar tectonic and climatic histories, the SSHCZO aims to quantify the role of lithology in the development and functioning of the critical zone. My research is based entirely at Garner Run.

This chapter summarizes my cosmogenic isotopic characterization of the residence time and erosion rate of soils, boulders, and stream sediments at Garner Run. I also report measurements from drill core samples that I prepared and measured, but the analysis and burial dating of these samples will be performed by Joanmarie Del Vecchio, a current M.S. student at Penn State.

Resistant sandstone ridgelines such as those at Garner Run are common features in the Ridge and Valley province of central Pennsylvania. My measurements demonstrate that sediment in small upland catchments such as Garner Run can have cosmogenic

nuclide concentrations equal to and exceeding the equivalent of 100 ka of surface exposure history. Despite perturbations by multiple glacial/interglacial cycles throughout the Pleistocene these sandstone-underlain environments are not young, and the exposure of surficial materials predates the last major advance of the Laurentide Ice Sheet at ~26 ka ago.

4.2 Introduction

4.2.1 *Geologic and physiographic setting*

Garner Run is a first-order, temperate forested sandstone subcatchment of the Shavers Creek watershed in the Ridge and Valley province of central Pennsylvania (Fig. 1), in the Susquehanna River Basin. The watershed is bounded by Tussey Mountain to the north and Leading Ridge to the south, both of which are underlain by the Tuscarora Formation, light to medium-gray Silurian arenitic sandstones (Berg et al., 1980). Leading Ridge is entirely forested whereas the ridgeline of Tussey Mountain is mantled by blocky colluvium and fractured bedrock outcrops in some places along the ridgeline. The structure of the catchment is controlled by the underlying Paleozoic rocks, and hillslopes reflect the 12-17° dip of the Tuscarora Formation (Brantley et al., 2016).

The landscape at Garner Run was repeatedly modified by periglacial activity over the course of the Pleistocene, when the Laurentide ice sheet extended within 100 km of the catchment at least 3 times (Braun, 1989, 2004; West et al., 2011), reaching its last maximum extent at ~26 ka (Corbett et al., 2016a). The geomorphology of the basin reflects these periods of periglaciation, with block fields (angular boulders <1 to 2 m) common on the surface of both slopes and relict solifluction lobes on Tussey Mountain

(visible in lidar imagery (Brantley et al., 2016; Del Vecchio, 2016)). Periglaciation is also reflected in the extensive valley fill in the floor of the catchment, where there is >9 m of sand interspersed with sandstone clasts (Brantley et al., 2016).

Garner Run is a low-gradient watershed with hillslopes that appear adjusted to the stream channel, but further downstream there are a series of breaks in the longitudinal stream profile, 'knickpoints' (Brantley et al., 2016). These knickpoints may reflect epiorogenic uplift over millions of years (Miller et al., 2013), stream capture (Willett et al., 2014), or heterogeneity of channel bedrock exposure (Cook et al., 2009). Knickpoints mark the transition between downstream areas of fluvial incision with higher erosion rates, and unincised relic landscapes upstream that remain unaffected. This wave of incision has already propagated up through the Shale Hills catchment, but has not yet translated through Garner Run.

4.2.2 *Cosmogenic Nuclides*

In-situ cosmogenic nuclides are produced in the uppermost several meters of rock and soil, where quartz grains are bombarded by secondary cosmic rays, primarily neutrons (Gosse and Phillips, 2001; Granger and Muzikar, 2001; Lal, 1998). Cosmogenic ^{10}Be and ^{26}Al are formed as a byproduct when cosmic rays strike ^{16}O and ^{28}Si, respectively (Lal, 1991). Cosmogenic isotopes are produced at the highest rate at Earth's surface. Production decreases with depth and production varies with elevation, latitude, and changes in Earth's magnetic field (Granger and Riebe, 2007; Lal, 1991; Nishiizumi et al., 1991).

There are three primary uses of cosmogenic nuclides—dating discrete bedrock surfaces, measuring erosion rates of bedrock outcrops (Lal, 1991), and measuring erosion rates at the drainage basin scale (Bierman and Steig, 1996; Brown et al., 1995; Granger et al., 1996). Cosmogenic nuclides in samples of bedrock can either be interpreted as an effective exposure age, the number over years of which the concentration of a nuclide would take to build up in a sample on the surface of the Earth, or as a steady state erosion rate. When measured in stream sediments, cosmogenic nuclides reflect spatially averaged erosion rates upstream of the sample site (Bierman and Steig, 1996; Brown et al., 1995; Granger et al., 1996). Accurate dating relies on a series of assumptions that are not always valid (Gosse and Phillips, 2001), including that the sample did not inherit nuclides from previous exposure (Bierman et al., 1999), and that there has been no erosion or cover by glaciers, soil, or other rocks.

When rocks are buried or shielded by other rocks for prolonged periods of time, their histories can be detected using two nuclides with different half-lives. This method most commonly uses ^{26}Al ($t_{1/2} = 0.71$) and ^{10}Be ($t_{1/2} = 1.38$), which are produced at a rate of approximately 7:1 (Argento et al., 2013; Corbett et al., 2016b; Nishiizumi et al., 2007; Nishiizumi et al., 1991). When a sample is buried the ^{26}Al/^{10}Be decreases, as ^{26}Al decays more rapidly than ^{10}Be. If a sample is re-exposed at the surface then production resumes, and the ratio increases.

4.2.3 *Previous Cosmogenic Work at the SSHCZO*

No prior cosmogenic work has been done at Garner Run; the most recent analysis of regolith residence time in Shavers Creek was by West et al. 2014, who used a suite of meteoric ^{10}Be samples used to quantify rates of landscape lowering at Shale Hills.

53

Meteoric [10]Be, unlike *in-situ*, is produced by spallation in the atmosphere, transported to the ground by rainfall, and adhered to grain coatings in sediment (McKean et al., 1993). Measurements of meteoric [10]Be at Shale Hills indicate that the landscape eroded at rates of ~20-30 m/My over the past 10-15 ka (West et al., 2014; West et al., 2011), that regolith predating ~15 ka may have been completely removed by periglacial forcing of the southern-facing ridgetop (Ma et al., 2013), and that transport rates depend on regolith depth, which is deeper on north-facing slopes. This marked asymmetry in hillslopes is likely from increased frequency of freeze-thaw events on southern facing slopes, which receive more exposure to sunlight than northern facing slopes do.

Meteoric and *in-situ* [10]Be are both used to calculate rates of landscape change, but they are two different systems. Production of *in*-situ [10]Be is well-constrained by our understanding of nuclear physics, whereas the sorption of meteoric [10]Be onto grain coatings is sometimes reversible, is controlled by geochemical processes, and can be dependent on grain size (Willenbring and Blanckenburg, 2010). Concentrations of meteoric and *in-situ* [10]Be in soils differ can dramatically with depth; Jungers et al. (2009) found meteoric [10]Be increased with depth and was correlated with aluminum concentrations, whereas *in-situ* concentrations were well-mixed through the soil column. Measurements of regolith residence times from these two systems are not directly comparable, as meteoric [10]Be represents the residence time of the mobile soil column, whereas *in-situ* accumulation incorporates the dosing of saprolite parent material before soil formation (Jungers et al., 2009).

4.3 Methods

4.3.1 *Sampling Strategy and Preparation*

I sampled boulders on three 30 m long transects adjacent to each of the 3 soil pits

on the top (GR07), middle (GR08), and bottom (GR09) of Leading Ridge. I centered a

measuring tape normal to the slope at each soil pit and removed the uppermost few

centimeters of rock from the nearest boulder on or about every 2 meters along the tape. I

sampled boulders representative of the typical boulder size on the slope (~1 m or less). I

collected 15 boulder chips for each transect, brought the pieces back to the lab, crushed

and sieved them individually, and added 50 g of each clast into a bag for amalgamation. I

also collected fluvial sediments (GR01 and GR02) ~15 m upstream and ~15 m

downstream from the bottommost Leading Ridge boulder transect, sieved each sample to

the 250-850 μm fraction, and washed out excess organic material upon returning to the

lab.

The remaining soil and drill core samples were sent to me from the SSHCZO

sample repository. The locations of all Garner Run samples are displayed in Figure 2.

The drill core clasts provided to me (*n* = 3) were small pieces of Tuscarora Formation

extracted from 3.3 m (sample GR10), 4.8 m (GR11), and 6.4 m (GR12) depth below the

valley floor. The SSHCZO soils (n=4) were extracted from soil pits dug at the top

(GR04), middle (GR05), and bottom (GR06) of Leading Ridge, as well as the middle of

Tussey Mountain (GR03), which is at a similar elevation as the top of Leading Ridge.

These pits were of variable depths, 0.7 m on Tussey Mountain, 0.65 m on Leading Ridge

ridgetop, 1.4 m Leading Ridge Midslope, and 1.4 m depth on the valley floor. I received

samples from each distinctive horizon (of different thicknesses), and to create a

representative sample for each soil pit I took 100g from each horizon, amalgamated all horizons, and sieved to the 250-850 μm sand fraction.

4.3.2 *Laboratory Work and Cosmogenic Nuclide Measurements*

I purified quartz at the University of Vermont (Kohl and Nishiizumi, 1992) and extracted ^{10}Be and ^{26}Al from the 250-850 μm fraction following the methods of Corbett et al. (2016a). All Garner Run samples were analyzed for ^{10}Be at Lawrence Livermore National Laboratory normalizing them relative to ICN standard 07KNSTD3110 with an assumed value of 2.85×10^{-12} (Nishiizumi et al., 2007). Samples GR01-GR09 were analyzed in April 2016, and GR10-12 in July 2016. We corrected GR01-GR09 using an average of n=3 process blanks ($6.43 \pm 2.00 \times 10^{-16}$) GR10-12 using an average of n=10 process blanks ($1.35 \pm 0.77 \times 10^{-15}$) (Table 1). We also sent the drill core samples (n=3) and the surface boulder transect samples (n=3) to PRIME lab (n=6) for ^{26}Al analysis. Exposure ages were calculated using the CRONUS-Earth online calculator (http://hess.ess.washington.edu/, wrapper script 2.2, main calculator 2.1, constants 2.2.1, see Balco et al. (2008)) based on the constant production rate model (Lal, 1991; Stone, 2000b) calibrated to the northeastern United States production rate (Balco et al., 2009).

4.4 Results

Measured ^{10}Be concentrations at Garner Run range from 2.27 ± 0.03 to 12.5 ± 0.27 x 10^5 atoms g^{-1} (Table 2), and the subset of ^{26}Al concentrations measurements in boulder and drill core samples range from 17.7 ± 0.87 to 73.97 ± 1.75 x 10^5 atoms g^{-1}.

The lowest ^{26}Al/^{10}Be ratio is 5.88 ± 0.28 in mid-drill core sample GR11, and the highest measured ratio is 7.79 ± 0.40 in mid-Leading Ridge boulder sample GR 08.

Leading Ridge ridgetop soils and boulders contain 2.90 ± 0.06 and 3.35 ± 0.08 x 10^5 atoms g^{-1} ^{10}Be, respectively. Leading Ridge valley floor soil and boulder concentrations are higher, 6.39 ± 0.07 and 8.26 ± 0.14 x 10^5 atoms g^{-1} (Fig. 3, 4). The average soil ^{10}Be concentration is 5.80 ± 2.81 x 10^5 atoms g^{-1}, and the average boulder concentration is 4.00 ± 2.13 x 10^5 atoms g^{-1}. Soil samples show a consistent increase downslope, whereas boulder concentrations are lower mid-slope than they are on the ridgetop. The one soil sample from Tussey Mountain (GR03) yields a ^{10}Be concentration of 7.93 ± 0.14 atoms g^{-1}, considerably higher than samples of similar elevation on Leading Ridge.

Nearby fluvial sediment samples GR01 and GR02 are consistent with soil and boulder measurements, containing an average of 5.94 ± 0.78 x 10^5 atoms g^{-1} ^{10}Be. This concentration represents an effective hillslope erosion rate of 6 m/My (Fig. 5). When converted into exposure ages the upper Leading Ridge rock and soil samples have 10Be concentrations equivalent to about 50 ka of exposure history. Rock and soil at the bottom of Leading Ridge contain ^{10}Be concentrations equivalent to over 100 ka of surface exposure (Table 2).

Drill core clasts (from top to bottom) contain 8.73 ± 0.15, 5.04 ± 0.09, and 125 ± 0.27 x 10^5 atoms g^{-1} ^{10}Be, respectively, and 5.68 ± 0.14, 2.96 ± 0.13, and 7.40 ± 1.75 x 10^6 atoms g^{-1} ^{26}Al (Fig. 6). The highest ^{10}Be and ^{26}Al concentrations of all samples measured at Garner Run are in the bottommost drill core sample, 6.4 m below the valley

floor. $^{26}Al/^{10}Be$ ratios from top to the bottom of the core are 6.5 ± 0.20, 5.88 ± 0.28, and 5.92 ± 0.19 (Fig. 7).

4.5 Discussion and Interpretation

Leading Ridge soil, stream sediment, and boulder samples have similar average ^{10}Be concentrations, 5.09 ± 2.82 (n=3), 5.95 ± 0.92 (n=2), and 4.01 ± 2.14 (n=3) x 10^5 atoms g^{-1}, respectively. These measurements are all within error of each other, and indicate that the detrital grains in the stream channel are representative of the average residence time of surficial materials upslope. This consistency leads us to believe that the measured fluvial erosion rate of 6m/My accurately represents the long-term lowering rate of this portion of the catchment.

An erosion rate of 6m/My is consistent with the bedrock arenite erosion rate in the Appalachian Moumtains of 5.9 ± 0.47 m/My (Portenga et al., 2013), but is lower than the regional fluvial erosion rate of 15 ± 3 m/My in relict sandstone landscapes above knickpoints in other areas of the Susquehanna River Basin (Miller et al., 2013). Low ridgeline erosion rates at Garner Run are consistent with Portenga et al. (2013) and Hancock and Kirwan (2007), who noted that ridgelines tend to erode at a slower pace than the regional fluvial network, which is incising into the landscape. However, this wave of incision has not yet propagated up through Garner Run. The extensive fill on the Garner Run valley floor indicates that hillslope denudation is faster the fluvial network's response, resulting in a net deposition of sediment.

The mid-slope Leading Ridge boulder transect contains less ^{10}Be than the ridgeline. This is counter to what we would expect, as regolith receives more cosmic ray dosing as

it moves downslope. Although our boulder amalgamation sampling strategy was designed to reduce the effects of clast heterogeneity, it likely did not eliminate it. Soils are composed of thousands of different grains, all of which have are sourced from different positions on the slope with different cosmic ray dosing histories. Grouped together, the quartz grains in soils are a much more effective representation of average upslope residence time than are individual clasts. Additionally, the mid-slope transect is at the foot of a steep lobe of boulders. Boulders that have recently been exhumed from the boulder lobe could also contribute to low [10]Be concentrations here.

The soil and boulder samples at Garner Run do not meet the assumptions for calculating *in-situ* cosmogenic exposure ages, as dating requires no erosion of the surface after exposure, no inheritance of nuclides at initial exposure, and no intermittent shielding or complex exposure history (i.e. by toppling or burial). However, if we regard measured [10]Be concentrations as minimum surface exposure times, then [10]Be concentrations on Leading Ridge represent ~50 ka of exposure and valley floor samples contain [10]Be concentrations equivalent to ~100 ka of continuous surface exposure. Despite glacial/interglacial cycles (Braun, 1989) sediment resides in the catchment over long timescales.

Shale Hills and Garner Run are only 3 km^2 apart and have similar climate histories, but they are underlain by different rock types and have different base level histories. The sandstone at Garner Run is well indurated and arenitic, whereas Shale Hills is underlain by weaker, more weathering-prone shale. Shale Hills has already been incised by the local wave of incision, whereas Garner Run remains a relict landscape. Combined, these factors make Garner Run a more stable environment. Our measurements confirm this

difference, as Garner Run *in-situ* [10]Be regolith residence times that are considerably longer than the ridgetop meteoric inventories at Shale Hills corresponding to ~10 ka of meteoric [10]Be accumulation (West et al., 2013). Though meteoric [10]Be and *in-situ* [10]Be are two separate isotopic systems and comparisons between the two dating methods cannot be made with precision, the 5 to 10x longer residence times at the top of the Leading Ridge slopes reflect differences beyond those inherent to these two different methods of tracing residence time and are thus likely real.

Ma et al. (2013) suggested that Shale Hills regolith younger than ~15 ka was completely removed from the upper and middle south-facing ridgetop due to severe erosion during periglaciation, but this suggestion is not supported by the data from Garner Run. There, the [10]Be concentration in soil from south-facing Tussey Mountain integrates the equivalent of > 100 ka of surface exposure.

The measured [10]Be in Tussey Mountain soil is higher than that of any other rock, soil, or sediment sample on the Leading Ridge side, yet with the solifluction lobes and periglacial features, one would expect concentrations on Tussey Mountain to be the lowest. With only one sample we do not have adequate data to assess aspect-dependency at Garner Run, or to determine whether nuclide concentration in soils is depth-dependent, as the Tussey Mountain pit (0.7 m) is shallower than those on Leading Ridge midslope and valley floor (both ~1.4 m).

The two-isotope plot of drill core samples shows that GR10 (3.4 m depth) plots close to the surface production ratio of ~7, whereas GR11 (4.9 m) and GR12 (6.4 m) have lower ratios, indicating burial sufficient for the ratio to lower from preferential decay of [26]Al (Fig. 7). GR12 has higher nuclide concentrations than any measured surface sample

and without accounting for decay contains nuclide concentrations equivalent to 216 ± 20 ka of exposure, but low ^{26}Al /^{10}Be ratios indicate that the sample has been buried for over 100 ka (as visible on the two-isotope diagram, Fig. 7). Overlying core samples GR10 (3.4 m) and GR11 (4.9 m) contain considerably less ^{10}Be, and without accounting for decay contain an equivalent of ~150 ka and ~80 of exposure, respectively. The variation in ratios and absolute concentrations in core samples is not consistent with gradual 'conveyor belt' transport downslope, rather it shows that regolith transport is heterogeneous over time and likely occurs in pulses.

In order to have such high nuclide concentrations sample GR12 (6.4 m) must have been within a meter of the surface for over 200 ka, indicating either a long period of landscape stability, or a long period of gradual downslope transport to the valley floor. The measured ^{10}Be/^{26}Al ratios in GR12 and GR11 core are consistent with burial times greater than 100 ka, and may indicate that they were moved to the valley floor at the same time, perhaps the penultimate glacial maximum (MIS 6, ~150 ka (Railsback et al., 2015)). However, the topmost clast (GR10) is close to the surface production ratio. It is possible that the deep deposit of sand overlying the clasts (Fig. 6) represents a sudden influx of material under periglaciation, and could be one of the solifluction lobes observed on Tussey Mountain, possibly from the Last Glacial Maximum. The alternating layers of sand and clasts in the core could represent periods of interglacial stability interspersed with period episodic transport under cold climate conditions.

Garner Run is a slowly evolving relic landscape that is in disequilibrium with downstream rates of landscape change. Measured ^{10}Be and ^{26}Al concentrations at Garner Run demonstrate that sandstone-underlain Appalachian headwater landscapes,

particularly those upstream of ongoing adjustments to base level, are remarkably stable and contain nuclide concentrations that pre-date the last glacial maximum. Cold weathering processes at the last glacial maximum were not enough to wipe out the 100+ ka of exposure history in hillslopes and sediments at Garner Run. Periglaciation at the LGM likely shaped the landscape at Garner Run, but it was not effective enough to renew the landscape entirely.

Figures
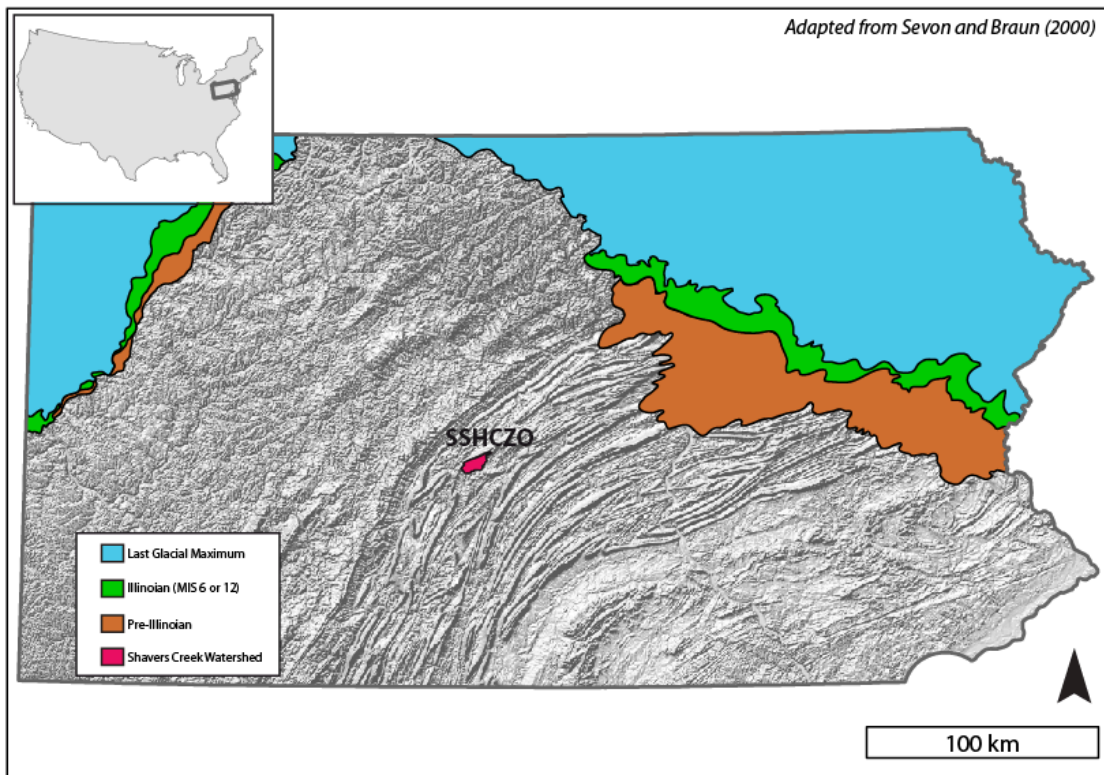
Figure 1. Location of Shavers Creek Watershed in relation to Pennsylvania glacial boundaries. Glacial map adapted from (Sevon and Braun, 2000)
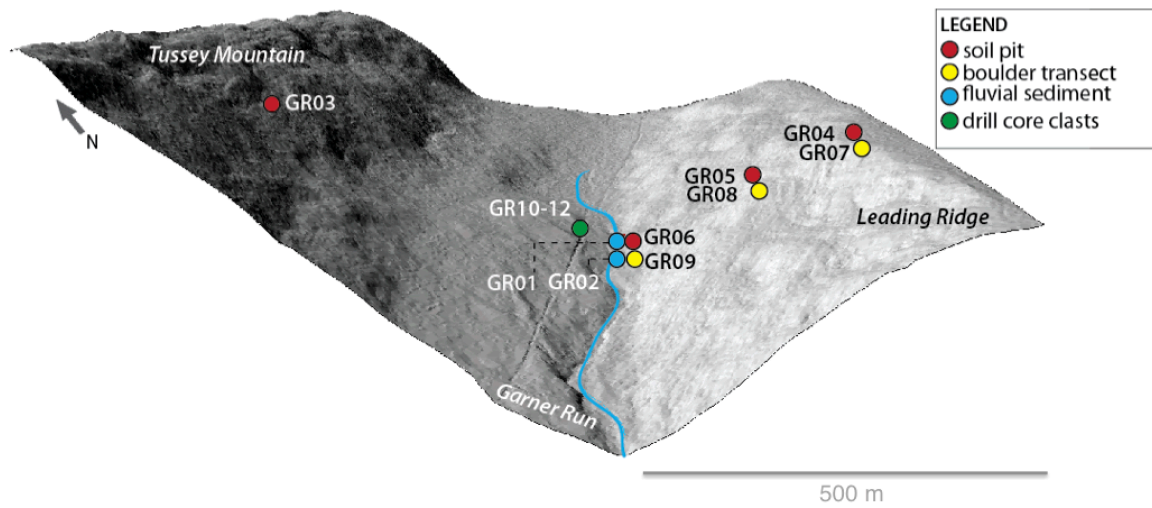
Figure 2. Location of sampling sites at Garner Run.
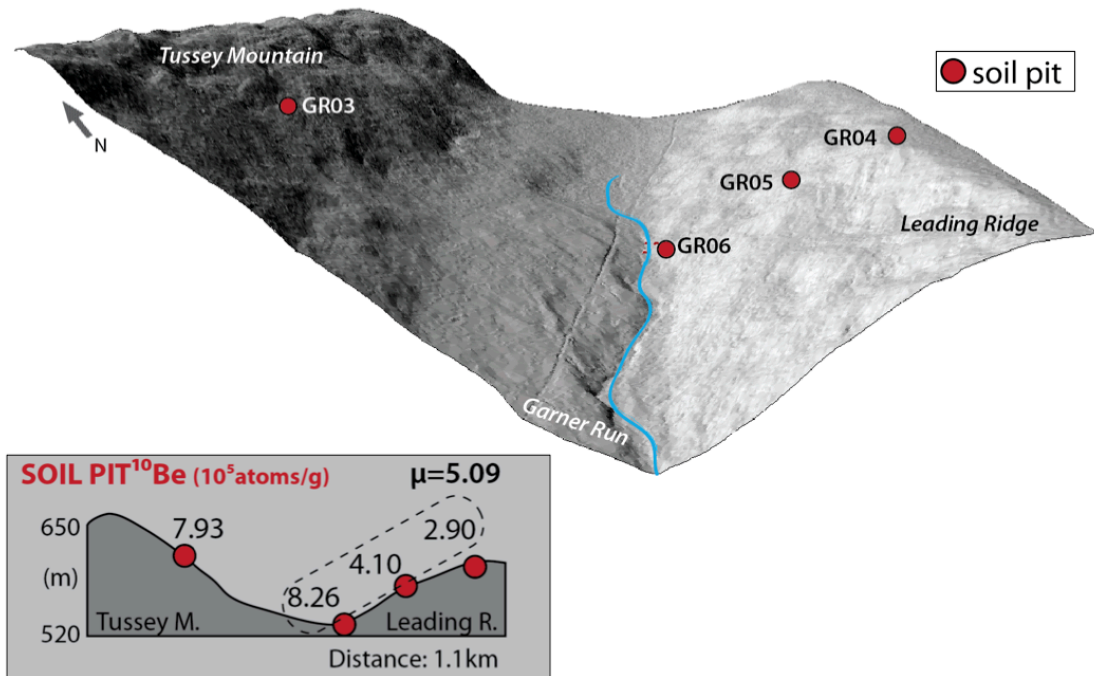
Figure 3. Locations and [10]Be concentrations of amalgamated soil pit samples.
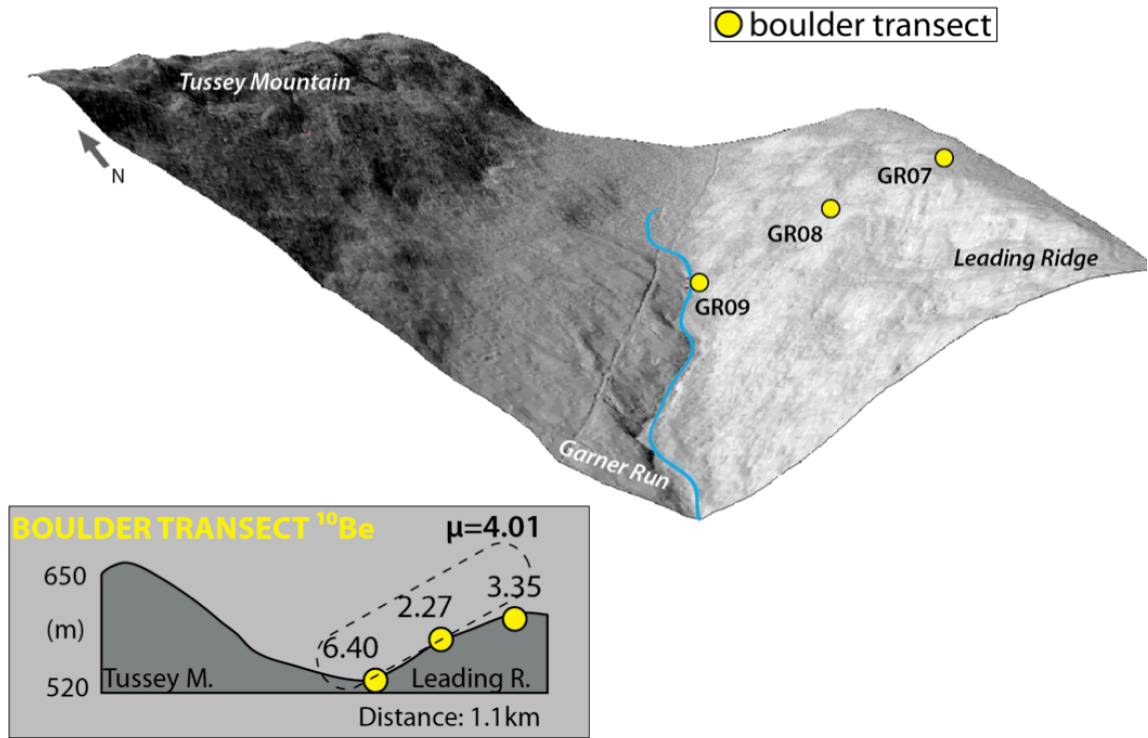
Figure 4. Locations and [10]Be concentrations of amalgamated boulder transect samples.
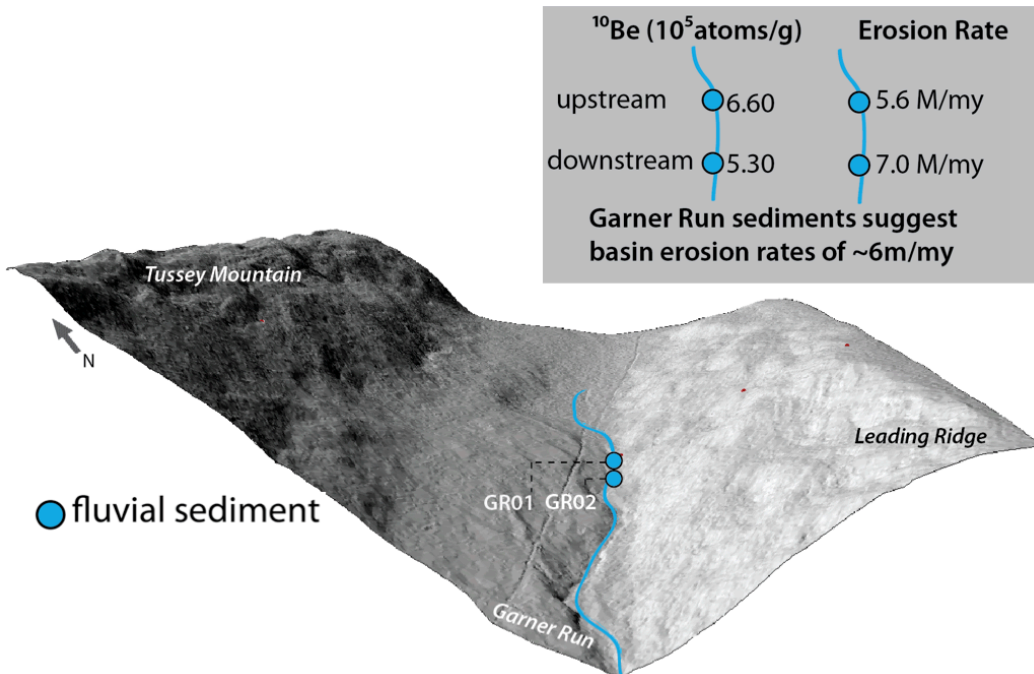
Figure 5. Locations, [10]Be concentrations, and erosion rates in fluvial sediment samples form Garner Run. Erosion rates average ~6m/My.
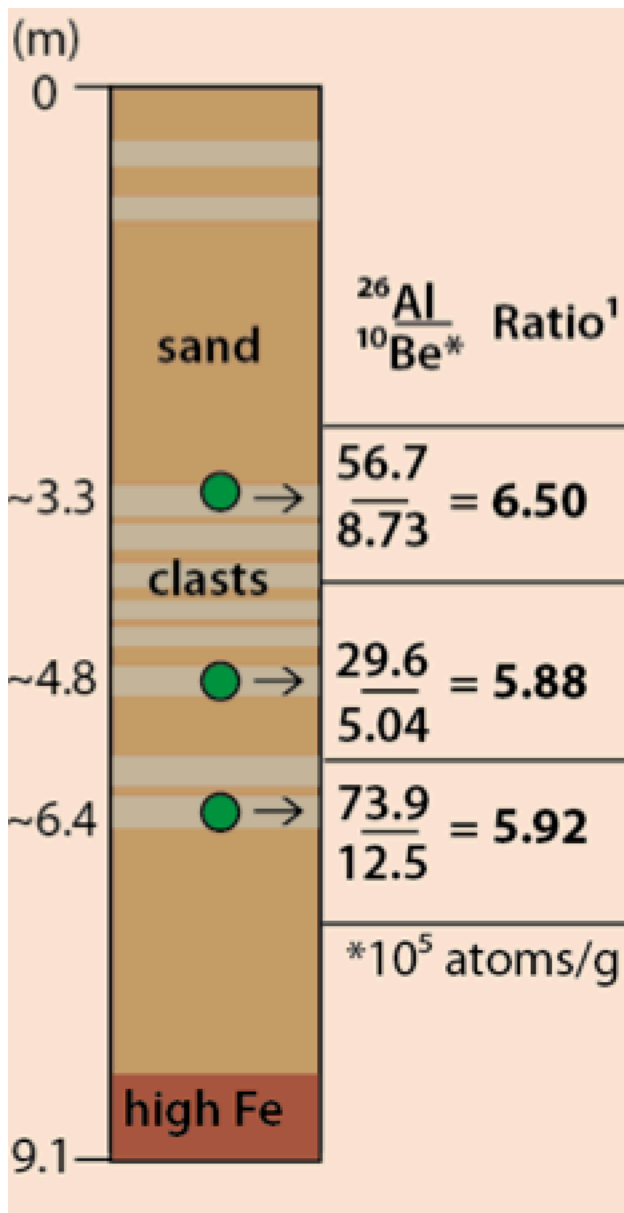
Figure 6. Layers of sediment within the Garner Run valley floor drill core, and the concentrations and ratios in measured clasts.
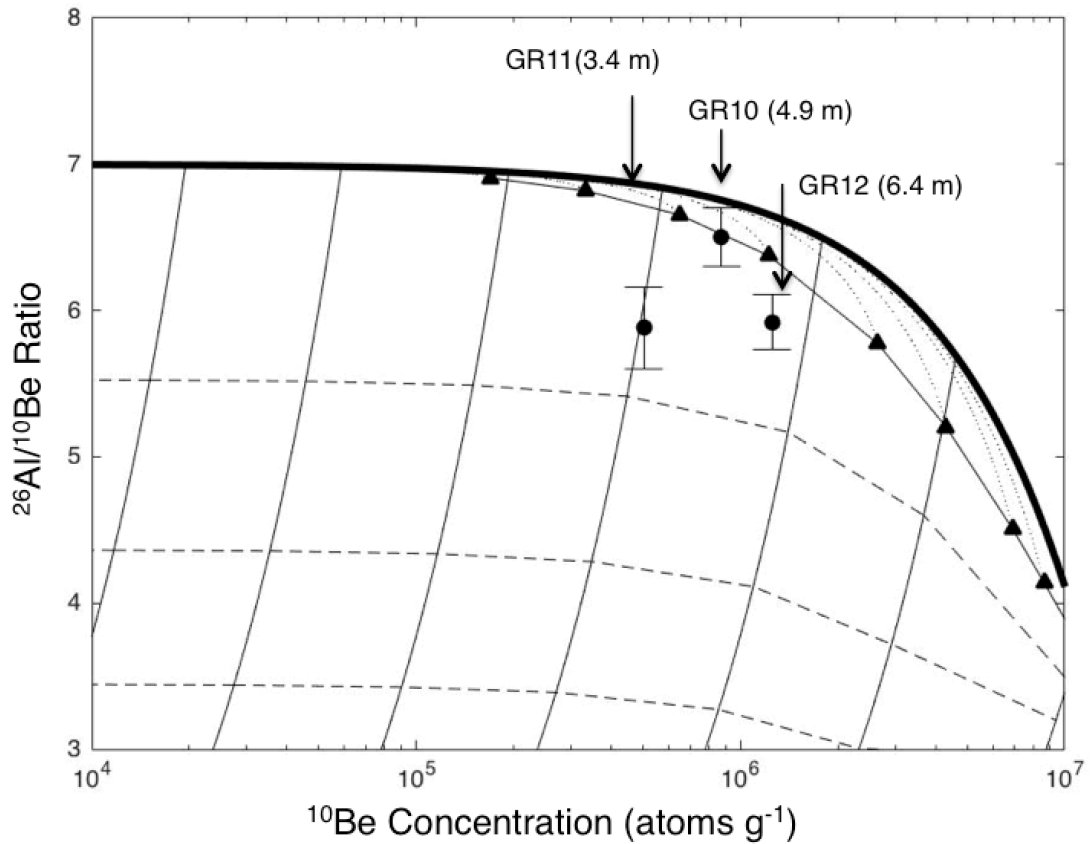
Figure 7. Two isotope plot of $^{26}Al/^{10}Be$ ratios vs ^{10}Be concentrations in drill core clasts. A sample with a simple exposure history (continuous exposure at the surface of the valley floor) will plot within the banana-shaped envelope at the top of the plot. Thick black line represents constant exposure at the surface, and the line beneath it marks the lowest a sample with a simple history can plot. Samples below this line have had at least one period of burial or shielding. Thin lines show the way path a sample would follow if buried, and horizontal dotted lines represent burial lines of 0.5, 1.0, and 1.5 m.y.. GR10 plots close to the surface whereas GR12 and GR11 have lower ratios.

Table 1. Laboratory preparation and AMS analysis information

Table 2. Sample attributes, location, and CRONUS results

Sample	Long. (°W)	Lat. (°N)	Elev. (masl)	Sample Type	10Be concentration (atoms/g)			26Al concentration (atoms/g)			26Al/10Be ratio			Erosion Rate (m/my)[1]			Exposure age (ka)[2]		
GR01	40.6961	-77.9213	501	upstream fluvial	6.60E+05	±	9.46E+03	n/a	±	n/a	n/a	±	n/a	5.56	±	0.48	113750	±	1680
GR02	40.6959	-77.9217	483	downstream fluvial	5.30E+05	±	6.14E+03	n/a	±	n/a	n/a	±	n/a	6.97	±	0.58	92220	±	1090
GR03	40.6997	-77.9246	575	Tussey soil	7.93E+05	±	1.37E+04	n/a	±	n/a	n/a	±	n/a	4.84	±	0.42	128970	±	2300
GR04	40.6939	-77.9190	586	LR ridge soil	2.90E+05	±	5.55E+03	n/a	±	n/a	n/a	±	n/a	14.5	±	1.17	45750	±	890
GR05	40.6949	-77.9199	555	LR mid soil	4.10E+05	±	5.41E+03	n/a	±	n/a	n/a	±	n/a	9.77	±	0.8	66680	±	900
GR06	40.6959	-77.9214	526	LR valley soil	8.26E+05	±	1.36E+04	n/a	±	n/a	n/a	±	n/a	4.44	±	0.39	140380	±	2400
GR07	40.6939	-77.9190	586	LR ridge rock	3.35E+05	±	8.15E+03	2.25E+06	±	1.18E+05	6.70	±	0.39	12.4	±	1.03	53010	±	1310
GR08	40.6949	-77.9199	555	LR mid rock	2.27E+05	±	2.73E+03	1.77E+06	±	8.73E+04	7.79	±	0.40	18.3	±	1.43	36700	±	450
GR09	40.6959	-77.9214	526	LR valley rock	6.40E+05	±	7.27E+03	3.87E+06	±	1.01E+05	6.05	±	0.17	5.88	±	0.5	107830	±	1260
GR10	40.6978	77.919	n/a	drill core 3.35 m	8.73E+05	±	1.47E+04	5.68E+06	±	1.41E+05	6.50	±	0.20	--	±	--	--	±	--
GR11	40.6978	77.919	n/a	drill core 4.87 m	5.04E+05	±	9.62E+03	2.96E+06	±	1.30E+05	5.88	±	0.28	--	±	--	--	±	--
GR12	40.6978	77.919	n/a	drill core 6.4 m	1.25E+06	±	2.71E+04	7.40E+06	±	1.75E+05	5.92	±	0.19	--	±	--	--	±	--

1. Erosion rates calculated using CRONUS calculator wrapper script version 2.3, calculator 2.1, function 2, constants 2.3, muons 1 using default calibration dataset.

2. Exposure ages calculated using CRONUS calculator (http://hess.ess.washington.edu/, wrapper script 2.2, main calculator 2.1, constants 2.2.1, see Balco et al. (2008)) based on the constant production rate model (Lal, 1991; Stone, 2000) calibrated to the northeastern United States production rate (Balco et al., 2009). `

Table 2. Sample location information and calculated exposure ages.

References

Argento, D. C., Reedy, R. C., and Stone, J. O., 2013, Modeling the Earth's cosmic radiation: Nuclear Instruments and Methods in Physics Research Section B: Beam Interactions with Materials and Atoms, v. 294, p. 464-469.

Balco, G., Briner, J., Finkel, R. C., Rayburn, J. A., Ridge, J. C., and Schaefer, J. M., 2009, Regional beryllium-10 production rate calibration for late-glacial northeastern North America: Quaternary Geochronology, v. 4, p. 93-107.

Balco, G., Stone, J. O., Lifton, N. A., and Dunai, T. J., 2008, A complete and easily accessible means of calculating surface exposure ages or erosion rates from [10]Be and [26]Al measurements: Quaternary Geochronology, v. 3, p. 174-195.

Baldwin, J. A., Whipple, K. X., and Tucker, G. E., 2003, Implications of the shear stress river incision model for the timescale of postorogenic decay of topography: Journal of Geophysical Research, v. 108, no. B3.

Berg, T., Edmunds, W., Geyer, A., Glover, A., Hoskins, D., MacLachlan, D., Root, S., Sevon, W., Socolow, A., and Miles, C., 1980, Geologic map of Pennsylvania: Pennsylvania Geological Survey, 4th Series, Map.

Bierman, P. R., Marsella, K. A., Patterson, C., Davis, P. T., and Caffee, M., 1999, Mid-Pleistocene cosmogenic minimum-age limits for pre-Wisconsinan glacial surfaces in southwestern Minnesota and southern Baffin Island; a multiple nuclide approach: Geomorphology, v. 27, no. 1-2, p. 25-39.

Bierman, P. R., and Steig, E., 1996, Estimating rates of denudation and sediment transport using cosmogenic isotope abundances in sediment: Earth Surface Processes and Landforms, v. 21, p. 125-139.

Boettcher, S. S., and Milliken, K. L., 1994, Mesozoic-Cenozoic unroofing of the southern Appalachian Basin: Apatite fission track evidence from Middle Pennsylvanian sandstones: The Journal of Geology, v. 102, no. 6, p. 655-668.

Brantley, S. L., DiBiase, R. A., Russo, T. A., Davis, K. J., Eissenstat, D. M., Dere, A. L., Neal, A. L., Brubaker, K. M., and Arthur, D. K., 2016, Designing a suite of measurements to understand the critical zone: Earth Surface Dynamics, v. 4, no. 1, p. 211.

Brantley, S. L., Goldhaber, M. B., and Ragnarsdottir, K. V., 2007, Crossing disciplines and scales to understand the critical zone: Elements, v. 3, no. 5, p. 307-314.

Braun, D. D., 1989, Glacial and Periglacial Erosion of the Appalachians: Geomorphology, v. 2, p. 233-256.

-, 2004, The glaciation of Pennsylvania, USA: Developments in Quaternary Sciences, v. 2, p. 237-242.

Brown, E. T., Stallard, R. F., Larsen, M. C., Raisbeck, G. M., and Yiou, F., 1995, Denudation rates determined from the accumulation of in situ-produced 10Be in the luquillo experimental forest, Puerto Rico: Earth and Planetary Science Letters, v. 129, p. 193-202.

Cook, K. L., Whipple, K. X., Heimsath, A. M., and Hanks, T. C., 2009, Rapid incision of the Colorado River in Glen Canyon–insights from channel profiles, local incision rates, and modeling of lithologic controls: Earth Surface Processes and Landforms, v. 34, no. 7, p. 994-1010.

Corbett, A. B., Bierman, P. R., Stone, B. D., Caffee, M. W., and Larsen, P. L., 2016a, Cosmogenic nuclide age estimate for Laurentide Ice Sheet recession from the terminal moraine, New Jersey, USA, and constraints on Latest Pleistocene ice sheet history: Quaternary Research, v. in review.

Corbett, L. B., Bierman, P. R., and Davis, P. T., 2016b, Glacial history and landscape evolution of southern Cumberland Peninsula, Baffin Island, Canada, constrained by cosmogenic [10]Be and [26]Al: Geological Society of America Bulletin, p. B31402. 31401.

Davis, W. M., 1899, The geographical cycle: Geographical Journal, v. 14, p. 481-504.

Del Vecchio, J., Surface and subsurface characteristics of periglacial landscape modification in central Pennsylvania, *in* Proceedings Geological Society of America Abstracts with ProgramsSeptember 25th, 2016 2016, Volume 48, No. 7.

Gallen, S. F., Wegmann, K. W., and Bohnenstiehl, D., 2013, Miocene rejuvenation of topographic relief in the southern Appalachians: GSA Today, v. 23, no. 2, p. 4-10.

Gosse, J. C., and Phillips, F. M., 2001, Terrestrial in situ cosmogenic nuclides: theory and application: Quaternary Science Reviews, v. 20, no. 14, p. 1475-1560.

Granger, D. E., Kirchner, J. W., and Finkel, R., 1996, Spatially averaged long-term erosion rates measured from in situ-produced cosmogenic nuclides in alluvial sediments: Journal of Geology, v. 104, no. 3, p. 249-257.

Granger, D. E., and Muzikar, P. F., 2001, Dating sediment burial with in situ-produced cosmogenic nuclides; theory, techniques, and limitations: Earth and Planetary Science Letters, v. 188, no. 1-2, p. 269-281.

Granger, D. E., and Riebe, C. S., 2007, Cosmogenic Nuclides in Weathering and Erosion, *in* Holland, H. D., and Turekian, K. K., eds., Treatise on Geochemistry: Oxford, Pergamon, p. 1-42.

Hack, J. T., 1960, Interpretation of erosional topography in humid temperate regions: American Journal of Science, v. 258A, p. 80-97.

Hancock, G., and Kirwan, M., 2007, Summit erosion rates deduced from 10Be: Implications for relief production in the central Appalachians: Geology, v. 35, no. 1, p. 89-92.

Jungers, M. C., Bierman, P. R., Matmon, A., Nichols, K., Larsen, J., and Finkel, R., 2009, Tracing hillslope sediment production and transport with in situ and meteoric [10]Be: Journal of Geophysical Research, v. 114, no. F04020, p. 1-16.

Kohl, C. P., and Nishiizumi, K., 1992, Chemical isolation of quartz for measurement of *in-situ* -produced cosmogenic nuclides: Geochimica et Cosmochimica Acta, v. 56, p. 3583-3587.

Lal, D., 1991, Cosmic ray labeling of erosion surfaces; in situ nuclide production rates and erosion models: Earth and Planetary Science Letters, v. 104, no. 2-4, p. 424-439.

-, 1998, Cosmic ray produced isotopes in terrestrial systems, *in* Goswami, J. N., and Krishnaswami, S., eds., Isotopes in the solar system; proceedings Proceedings of the Indian Academy of Sciences, Indian Academy of Sciences, Bangalore, India, p. Earth and Planetary Sciences 107, no. 104 (199812) 199241-199249.

Liu, L., 2014, Rejuvenation of Appalachian topography caused by subsidence-induced differential erosion: Nature Geosci, v. 7, no. 7, p. 518-523.

Ma, L., Chabaux, F., West, N., Kirby, E., Jin, L., and Brantley, S., 2013, Regolith production and transport in the Susquehanna Shale Hills Critical Zone Observatory, Part 1: Insights from U‐series isotopes: Journal of Geophysical Research: Earth Surface, v. 118, no. 2, p. 722-740.

McKean, J. A., Dietrich, W. E., Finkel, R. C., Southon, J. R., and Caffee, M. W., 1993, Quantification of soil production and downslope creep rates from cosmogenic [10]Be accumulations on a hillslope profile: Geology, v. 21, no. 4, p. 343-346.

Miller, S. R., Sak, P. B., Kirby, E., and Bierman, P. R., 2013, Neogene rejuvenation of central Appalachian topography: Evidence for differential rock uplift from stream profiles and erosion rates: Earth and Planetary Science Letters, v. 369, p. 1-12.

Nishiizumi, K., Imamura, M., Caffee, M. W., Southon, J. R., Finkel, R. C., and McAninch, J., 2007, Absolute calibration of ^{10}Be AMS standards: Nuclear Inst. and Methods in Physics Research, B, v. 258, no. 2, p. 403-413.

Nishiizumi, K., Kohl, C. P., Arnold, J. R., Klein, J., Fink, D., and Middleton, R., 1991, Cosmic ray produced ^{10}Be and ^{26}Al in Antarctic rocks; exposure and erosion history: Earth and Planetary Science Letters, v. 104, no. 2-4, p. 440-454.

Pazzaglia, F., and Gardner, T., 1993, Fluvial terraces of the lower Susquehanna River: Geomorphology, v. 8, p. 83-113.

Pazzaglia, F. J., Braun, D. D., Pavich, M., Bierman, P., Potter Jr, N., Merritts, D., Walter, R., and Germanoski, D., 2006, Rivers, glaciers, landscape evolution, and active tectonics of the central Appalachians, Pennsylvania and Maryland, *in* Pazzaglia, F. J., ed., Excursions in Geology and History: Field Trips in the Middle Atlantic States: Geological Society of America Field Guide 8: Denver, GSA, p. 169-197.

Portenga, E. W., Bierman, P. R., Rizzo, D. M., and Rood, D. H., 2013, Low rates of bedrock outcrop erosion in the central Appalachian Mountains inferred from *in situ* ^{10}Be concentrations: Geological Society of America Bulletin, v. 125, no. 1-2, p. 201-215.

Prince, P. S., and Spotila, J. A., 2013, Evidence of transient topographic disequilibrium in a landward passive margin river system: knickpoints and paleo‐landscapes of the New River basin, southern Appalachians: Earth Surface Processes and Landforms, v. 38, no. 14, p. 1685-1699.

Railsback, L. B., Gibbard, P. L., Head, M. J., Voarintsoa, N. R. G., and Toucanne, S., 2015, An optimized scheme of lettered marine isotope substages for the last 1.0 million years, and the climatostratigraphic nature of isotope stages and substages: Quaternary Science Reviews, v. 111, p. 94-106.

Sevon, W. D., and Braun, D. D., 2000, Map 59: Glacial deposits of Pennsylvania, Pennsylvania Department of Conservation and Natural Resources Bureau of Topographic and Geologic Survey.

Stone, J. O., 2000, Cosmogenic isotope constraints on geomorphic processes and landscape evolution: Fission track 2000; 9th international conference on fission track dating and thermochronology Abstracts - Geological Society of Australia, v. 58, p. 309-310.

West, N., Kirby, E., Bierman, P., and Clarke, B. A., 2014, Aspect-dependent variations in regolith creep revealed by meteoric 10Be: Geology, v. 42, no. 6, p. 507-510.

West, N., Kirby, E., Bierman, P., and Rood, D., 2011, Preliminary estimates of regolith generation and mobility in the Susquehanna Shale Hills Critical Zone Observatory, Pennsylvania, using meteoric 10 Be: Applied Geochemistry, v. 26, p. S146-S148.

West, N., Kirby, E., Bierman, P., Slingerland, R., Ma, L., Rood, D., and Brantley, S., 2013, Regolith production and transport at the Susquehanna Shale Hills Critical Zone Observatory, part 2: insights from meteoric 10Be: Journal of Geophysical Research: Earth Surface, v. 118, no. 3, p. 1877-1896.

Willenbring, J. K., and Blanckenburg, F. v., 2010, Meteoric cosmogenic Beryllium-10 adsorbed to river sediment and soil: Applications for Earth-surface dynamics: Earth-Science Reviews, v. 98, p. 105-122.

Willett, S. D., McCoy, S. W., Perron, J. T., Goren, L., and Chen, C.-Y., 2014, Dynamic reorganization of river basins: Science, v. 343, no. 6175, p. 1248765.

CONCLUSIONS

Analyses of *in-situ* cosmogenic ^{10}Be and ^{26}Al can elucidate rates of landscape change in formerly glaciated and periglaciated landscapes. My isotopic data show that landscape evolution in Pennsylvannia fits two endmembers. The first is at Hickory Run and Garner Run, where I observe slowly eroding upland landscapes that have persisted on time scales of hundreds of thousands of years. The second is at Young Womans Creek, where perturbations to base level induce erosion rates that are up to 6x faster than those observed in slowly eroding upland catchments.

My findings add nuance to the conventional view of periglaciation as a force that 'wiped the slate clean' in the Appalachian Mountains, and shed light on the role of lithology in modulating base level change. I find that in upland areas with resistant lithologies, the landscape was reworked, but not reset by repeated periglaciation. All surficial materials dated in this thesis predate the Last Glacial Maximum at 26 ka. Additionally, my results demonstrate the effects of lithology and base level on erosion rate are difficult to disentangle, and that when studied on a small scale, lithology exerts the strongest control over the spatial variability of erosion in a transient landscape. The landscape in Pennsylvania is not in equilibrium, it is split between slowly eroding upland relict landscapes, and downstream areas that are rapidly responding to base level change.

COMPREHENSIVE BIBLIOGRAPHY

André, M.-F., Hall, K., Bertran, P., and Arocena, J., 2008, Stone runs in the Falkland Islands: Periglacial or tropical?: Geomorphology, v. 95, no. 3, p. 524-543.

Argento, D. C., Reedy, R. C., and Stone, J. O., 2013, Modeling the Earth's cosmic radiation: Nuclear Instruments and Methods in Physics Research Section B: Beam Interactions with Materials and Atoms, v. 294, p. 464-469.

Balco, G., Briner, J., Finkel, R. C., Rayburn, J. A., Ridge, J. C., and Schaefer, J. M., 2009, Regional beryllium-10 production rate calibration for late-glacial northeastern North America: Quaternary Geochronology, v. 4, p. 93-107.

Balco, G., and Rovey, C. W., 2008, An Isochron Method for Cosmogenic-nuclide Dating of Buried Soils and Sediments: American Journal of Science, v. 308, p. 1083-1114.

Balco, G., and Shuster, D. L., 2009, ^{26}Al–^{10}Be–^{21}Ne burial dating: Earth and Planetary Science Letters, v. 286, p. 570-575.

Balco, G., Stone, J. O., Lifton, N. A., and Dunai, T. J., 2008, A complete and easily accessible means of calculating surface exposure ages or erosion rates from ^{10}Be and ^{26}Al measurements: Quaternary Geochronology, v. 3, p. 174-195.

Baldwin, J. A., Whipple, K. X., and Tucker, G. E., 2003, Implications of the shear stress river incision model for the timescale of postorogenic decay of topography: Journal of Geophysical Research, v. 108, no. B3.

Barrows, T. T., Stone, J. O., and Fifield, L. K., 2004, Exposure ages for Pleistocene periglacial deposits in Australia: Quaternary Science Reviews, v. 23, no. 5-6, p. 697-708.

Beel, C., Lifton, N., Briner, J., and Goehring, B., 2016, Quaternary evolution and ice sheet history of contrasting landscapes in Uummannaq and Sukkertoppen, western Greenland: Quaternary Science Reviews, v. 149, p. 248-258.

Berg, T., Edmunds, W., Geyer, A., Glover, A., Hoskins, D., MacLachlan, D., Root, S., Sevon, W., Socolow, A., and Miles, C., 1980, Geologic map of Pennsylvania: Pennsylvania Geological Survey, 4th Series, Map.

Berg, T. M., 1979, The Huntley Mountain Formation: Catskill-to-Burgoon transition in north-central Pennsylvania, Department of Environmental Resources, Bureau of Topographic and Geologic Survey, v. 83.

Bierman, P. R., Davis, P. T., Corbett, L. B., Lifton, N. A., and Finkel, R. C., 2015, Cold-based Laurentide ice covered New England's highest summits during the Last Glacial Maximum: Geology, v. 43, no. 12, p. 1059-1062.

Bierman, P. R., Marsella, K. A., Patterson, C., Davis, P. T., and Caffee, M., 1999, Mid-Pleistocene cosmogenic minimum-age limits for pre-Wisconsinan glacial surfaces in southwestern Minnesota and southern Baffin Island; a multiple nuclide approach: Geomorphology, v. 27, no. 1-2, p. 25-39.

Bierman, P. R., and Steig, E., 1996, Estimating rates of denudation and sediment transport using cosmogenic isotope abundances in sediment: Earth Surface Processes and Landforms, v. 21, p. 125-139.

Boelhouwers, J., Holness, S., Meiklejohn, I., and Sumner, P., 2002, Observations on a blockstream in the vicinity of Sani Pass, Lesotho Highlands, southern Africa: Permafrost and Periglacial Processes, v. 13, no. 4, p. 251-257.

Boettcher, S. S., and Milliken, K. L., 1994, Mesozoic-Cenozoic unroofing of the southern Appalachian Basin: Apatite fission track evidence from Middle Pennsylvanian sandstones: The Journal of Geology, v. 102, no. 6, p. 655-668.

Brantley, S. L., DiBiase, R. A., Russo, T. A., Davis, K. J., Eissenstat, D. M., Dere, A. L., Neal, A. L., Brubaker, K. M., and Arthur, D. K., 2016, Designing a suite of measurements to understand the critical zone: Earth Surface Dynamics, v. 4, no. 1, p. 211.

Brantley, S. L., Goldhaber, M. B., and Ragnarsdottir, K. V., 2007, Crossing disciplines and scales to understand the critical zone: Elements, v. 3, no. 5, p. 307-314.

Braun, D. D., 1989, Glacial and Periglacial Erosion of the Appalachians: Geomorphology, v. 2, p. 233-256.

-, 2004, The glaciation of Pennsylvania, USA: Developments in Quaternary Sciences, v. 2, p. 237-242.

Brown, E. T., Stallard, R. F., Larsen, M. C., Raisbeck, G. M., and Yiou, F., 1995, Denudation rates determined from the accumulation of in situ-produced 10Be in the luquillo experimental forest, Puerto Rico: Earth and Planetary Science Letters, v. 129, p. 193-202.

Castillo, M., Bishop, P., and Jansen, J. D., 2013, Knickpoint retreat and transient bedrock channel morphology triggered by base-level fall in small bedrock river catchments: The case of the Isle of Jura, Scotland: Geomorphology, v. 180, p. 1-9.

Chmeleff, J., Blanckenburg, F. v., Kossert, K., and Jakob, D., 2009, Determination of the ^{10}Be half-life by multicollector ICP-MS and liquid scintillation counting: Nuclear Instruments and Methods in Physics Research Section B: Beam Interactions with Materials and Atoms, v. 268, no. 2, p. 192-199.

Clark, G. M., and Ciolkosz, E. J., 1988, Periglacial geomorphology of the Appalachian Highlands and Interior Highlands south of the glacial border—a review: Geomorphology, v. 1, no. 3, p. 191-220.

Colgan, P. M., Bierman, P. R., Mickelson, D. M., and Caffee, M., 2002, Variation in glacial erosion near the southern margin of the Laurentide Ice Sheet, south-central Wisconsin, USA: Implications for cosmogenic dating of glacial terrains: Geological Society of America Bulletin, v. 114, no. 12, p. 1581-1591.

Colton, G. W., and Luft, S. J., 1965, Bedrock Geology of the Slate Run Quadrangle, Clinton, Lycoming, and Potter Counties, Pennsylvania, Commonwealth of Pennsylvania, Department of Internal Affairs, Bureau of Topographic and Geological Survey.

Cook, K. L., Whipple, K. X., Heimsath, A. M., and Hanks, T. C., 2009, Rapid incision of the Colorado River in Glen Canyon–insights from channel profiles, local incision rates, and modeling of lithologic controls: Earth Surface Processes and Landforms, v. 34, no. 7, p. 994-1010.

Corbett, A. B., Bierman, P. R., Stone, B. D., Caffee, M. W., and Larsen, P. L., 2016a, Cosmogenic nuclide age estimate for Laurentide Ice Sheet recession from the

terminal moraine, New Jersey, USA, and constraints on Latest Pleistocene ice
sheet history: Quaternary Research, v. in review.

Corbett, L. B., Bierman, P. R., and Davis, P. T., 2016b, Glacial history and landscape
evolution of southern Cumberland Peninsula, Baffin Island, Canada, constrained
by cosmogenic [10]Be and [26]Al: Geological Society of America Bulletin, p. B31402.
31401.

Corbett, L. B., Bierman, P. R., and Rood, D. H., 2016c, An approach for optimizing in
situ cosmogenic 10 Be sample preparation: Quaternary Geochronology, v. 33, p.
24-34.

Crosby, B. T., and Whipple, K. X., 2006, Knickpoint initiation and distribution within
fluvial networks: 236 waterfalls in the Waipaoa River, North Island, New
Zealand: Geomorphology, v. 82, no. 1-2, p. 16-38.

Cyr, A. J., Granger, D. E., Olivetti, V., and Molin, P., 2014, Distinguishing between
tectonic and lithologic controls on bedrock channel longitudinal profiles using
cosmogenic 10Be erosion rates and channel steepness index: Geomorphology, v.
209, p. 27-38.

Davis, W. M., 1889, The Rivers and Valleys of Pennsylvania: National Geographic
Magazine, v. 1, no. 3, p. 183-253.

Davis, W. M., 1899, The geographical cycle: Geographical Journal, v. 14, p. 481-504.

Del Vecchio, J., Surface and subsurface characteristics of periglacial landscape
modification in central Pennsylvania, in Proceedings Geological Society of
America Abstracts with ProgramsSeptember 25th, 2016 2016, Volume 48, No. 7.

Firpo, M., Guglielmin, M., and Queirolo, C., 2006, Relict blockfields in the ligurian alps
(Mount Beigua, Italy): Permafrost and Periglacial Processes, v. 17, no. 1, p. 71-
78.

French, H. M., and Millar, S. W., 2014, Permafrost at the time of the Last Glacial
Maximum (LGM) in North America: Boreas, v. 43, no. 3, p. 667-677.

Gallen, S. F., Wegmann, K. W., and Bohnenstiehl, D., 2013, Miocene rejuvenation of
topographic relief in the southern Appalachians: GSA Today, v. 23, no. 2, p. 4-10.

Gosse, J. C., and Phillips, F. M., 2001, Terrestrial in situ cosmogenic nuclides: theory and
application: Quaternary Science Reviews, v. 20, no. 14, p. 1475-1560.

Granger, D. E., Kirchner, J. W., and Finkel, R., 1996, Spatially averaged long-term
erosion rates measured from in situ-produced cosmogenic nuclides in alluvial
sediments: Journal of Geology, v. 104, no. 3, p. 249-257.

Granger, D. E., and Muzikar, P. F., 2001, Dating sediment burial with in situ-produced
cosmogenic nuclides; theory, techniques, and limitations: Earth and Planetary
Science Letters, v. 188, no. 1-2, p. 269-281.

Granger, D. E., and Riebe, C. S., 2007, Cosmogenic Nuclides in Weathering and Erosion,
in Holland, H. D., and Turekian, K. K., eds., Treatise on Geochemistry: Oxford,
Pergamon, p. 1-42.

Hack, J. T., 1957, Studies of longitudinal stream profiles in Virginia and Maryland, US
Government Printing Office.

Hack, J. T., 1960, Interpretation of erosional topography in humid temperate regions:
American Journal of Science, v. 258A, p. 80-97.

-, 1975, Dynamic equilibrium and landscape evolution, *in* Melhorn, W. N., and Flemal, R. C., eds., Theories of landform development: Binghamton, N.Y., SUNY Binghamton,, p. 87-102.

Hancock, G., and Kirwan, M., 2007, Summit erosion rates deduced from 10Be: Implications for relief production in the central Appalachians: Geology, v. 35, no. 1, p. 89-92.

Howard, A. D., Dietrich, W. E., and Seidl, M. A., 1994, Modeling fluvial erosion on regional to continental scales: Journal of Geophysical Research, B, Solid Earth and Planets, v. 99, no. 7, p. 13,971-913,986.

Isaaks, E. H., and Srivastava, R. M., 1989, Applied geostatistics: Oxford University Press: New York, p. 561.

Journel, A. G., and Huijbregts, C. J., 1978, Mining geostatistics, Academic press.

Joyce, J. R., 1950, Stone runs of the Falkland Islands: Geological Magazine, v. 87, no. 2, p. 105-115.

Jungers, M. C., Bierman, P. R., Matmon, A., Nichols, K., Larsen, J., and Finkel, R., 2009, Tracing hillslope sediment production and transport with in situ and meteoric [10]Be: Journal of Geophysical Research, v. 114, no. F04020, p. 1-16.

Kirby, E., and Whipple, K. X., 2012, Expression of active tectonics in erosional landscapes: Journal of Structural Geology, v. 44, p. 54-75.

Kleman, J., and Borgström, I., 1990, The boulder fields of Mt. Fulufjället, west-central Sweden-Late Weichselian boulder blankets and interstadial periglacial phenomena: Geografiska Annaler. Series A. Physical Geography, p. 63-78.

Kohl, C. P., and Nishiizumi, K., 1992, Chemical isolation of quartz for measurement of *in-situ* -produced cosmogenic nuclides: Geochimica et Cosmochimica Acta, v. 56, p. 3583-3587.

Korschinek, G., Bergmaier, A., Faestermann, T., Gerstmann, U. C., Knie, K., Rugel, G., Wallner, A., Dillmann, I., Dollinger, G., Gostomski, C. L. v., Kossert, K., Maiti, M., Poutivtsev, M., and Remmert, A., 2010, A new value for the half-life of 10Be by Heavy-Ion Elastic Recoil Detection and liquid scintillation counting: Nuclear Instruments and Methods in Physics Research B, v. 268, p. 187-191.

Lal, D., 1991, Cosmic ray labeling of erosion surfaces; in situ nuclide production rates and erosion models: Earth and Planetary Science Letters, v. 104, no. 2-4, p. 424-439.

-, 1998, Cosmic ray produced isotopes in terrestrial systems, *in* Goswami, J. N., and Krishnaswami, S., eds., Isotopes in the solar system; proceedings Proceedings of the Indian Academy of Sciences, Indian Academy of Sciences, Bangalore, India, p. Earth and Planetary Sciences 107, no. 104 (199812) 199241-199249.

Lambeck, K., Rouby, H., Purcell, A., Sun, Y., and Sambridge, M., 2014, Sea level and global ice volumes from the Last Glacial Maximum to the Holocene: Proceedings of the National Academy of Sciences, v. 111, no. 43, p. 15296-15303.

Liu, L., 2014, Rejuvenation of Appalachian topography caused by subsidence-induced differential erosion: Nature Geosci, v. 7, no. 7, p. 518-523.

Ma, L., Chabaux, F., West, N., Kirby, E., Jin, L., and Brantley, S., 2013, Regolith production and transport in the Susquehanna Shale Hills Critical Zone

Observatory, Part 1: Insights from U‑series isotopes: Journal of Geophysical Research: Earth Surface, v. 118, no. 2, p. 722-740.

McKean, J. A., Dietrich, W. E., Finkel, R. C., Southon, J. R., and Caffee, M. W., 1993, Quantification of soil production and downslope creep rates from cosmogenic [10]Be accumulations on a hillslope profile: Geology, v. 21, no. 4, p. 343-346.

Miller, S. R., Sak, P. B., Kirby, E., and Bierman, P. R., 2013, Neogene rejuvenation of central Appalachian topography: Evidence for differential rock uplift from stream profiles and erosion rates: Earth and Planetary Science Letters, v. 369, p. 1-12.

Mills, H. H., 2000, Apparent Increasing Rates of Stream Incision in the Eastern United States During the Late Cenozoic: Geology, v. 28, no. 10, p. 955-957.

Nelson, K. J. P., Nelson, F. E., and Walegur, M. T., 2007, Periglacial Appalachia: palaeoclimatic significance of blockfield elevation gradients, eastern USA: Permafrost and Periglacial Processes, v. 18, no. 1, p. 61-73.

Nishiizumi, K., Imamura, M., Caffee, M. W., Southon, J. R., Finkel, R. C., and McAninch, J., 2007, Absolute calibration of [10]Be AMS standards: Nuclear Inst. and Methods in Physics Research, B, v. 258, no. 2, p. 403-413.

Nishiizumi, K., Kohl, C. P., Arnold, J. R., Dorn, R., Klein, J., Fink, D., Middleton, R., and Lal, D., 1993, Role of in situ cosmogenic nuclides [10]Be and [26]Al in the study of diverse geomorphic processes: Earth Surface Processes and Landforms, v. 18, no. 5, p. 407-425.

Nishiizumi, K., Kohl, C. P., Arnold, J. R., Klein, J., Fink, D., and Middleton, R., 1991, Cosmic ray produced [10]Be and [26]Al in Antarctic rocks; exposure and erosion history: Earth and Planetary Science Letters, v. 104, no. 2-4, p. 440-454.

NRCS, 2014, Soil Survey Geographic database for Pennsylvania: Forth Worth, Texas, U.S. Department of Agriculture, Natural Resources Conservation Sevice.

Pazzaglia, F., and Gardner, T., 1993, Fluvial terraces of the lower Susquehanna River: Geomorphology, v. 8, p. 83-113.

Pazzaglia, F. J., and Brandon, M. T., 1996, Macrogeomorphic evolution of the post-Triassic Appalachian mountains determined by deconvolution of the offshore basin sedimentary record: Basin Research, v. 8, no. 255-278.

Pazzaglia, F. J., Braun, D. D., Pavich, M., Bierman, P., Potter Jr, N., Merritts, D., Walter, R., and Germanoski, D., 2006, Rivers, glaciers, landscape evolution, and active tectonics of the central Appalachians, Pennsylvania and Maryland, *in* Pazzaglia, F. J., ed., Excursions in Geology and History: Field Trips in the Middle Atlantic States: Geological Society of America Field Guide 8: Denver, GSA, p. 169-197.

Péwé, T. L., 1983, The periglacial environment in North America during Wisconsin time: Late-quaternary environments of the United States, v. 1, p. 157-189.

Portenga, E. W., Bierman, P. R., Rizzo, D. M., and Rood, D. H., 2013, Low rates of bedrock outcrop erosion in the central Appalachian Mountains inferred from *in situ* [10]Be concentrations: Geological Society of America Bulletin, v. 125, no. 1-2, p. 201-215.

Potter, N., and Moss, J. H., 1968, Origin of the Blue Rocks block field and adjacent deposits, Berks County, Pennsylvania: Geological Society of America Bulletin, v. 79, no. 2, p. 255-262.

Prince, P. S., and Spotila, J. A., 2013, Evidence of transient topographic disequilibrium in a landward passive margin river system: knickpoints and paleo‐landscapes of the New River basin, southern Appalachians: Earth Surface Processes and Landforms, v. 38, no. 14, p. 1685-1699.

Psilovikos, A., and Van Houten, F., 1982, Ringing rocks barren block field, east-central Pennsylvania: Sedimentary Geology, v. 32, no. 3, p. 233-243.

Railsback, L. B., Gibbard, P. L., Head, M. J., Voarintsoa, N. R. G., and Toucanne, S., 2015, An optimized scheme of lettered marine isotope substages for the last 1.0 million years, and the climatostratigraphic nature of isotope stages and substages: Quaternary Science Reviews, v. 111, p. 94-106.

Riebe, C. S., Kirchner, J. W., Granger, D. E., and Finkel, R. C., 2000, Erosional equilibrium and disequilibrium in the Sierra Nevada, inferred from cosmogenic ^{26}Al and ^{10}Be in alluvial sediment: Geology, v. 28, no. 9, p. 803-806.

Seong, Y. B., and Kim, J. W., 2003, Application of In-situ Produced Cosmogenic ^{10}Be and ^{26}Al for Estimating Erosion Rate and Exposure Age of Tor and Block Stream Detritus: Case Study from Mt. Maneo, South Korea: Journal of Korean Geographical Society, v. 38, no. 3, p. 389-399.

Sevon, W. D., 1975, Geology and mineral resources of the Hickory Run and Blakeslee quadrangles, Carbon and Monroe Counties, Pennsylvania, Commonwealth of Pennsylvania, Department of Environmental Resources, Bureau of Topographic and Geologic Survey.

Sevon, W. D., 2000, Map 13: Physiographic Provinces of Pennsylvania: Commonwealth of Pennsylvania Department of Conservation and Natural Resources Bureau of Topographic and Geologic Survey.

Sevon, W. D., and Braun, D. D., 2000, Map 59: Glacial deposits of Pennsylvania, Pennsylvania Department of Conservation and Natural Resources Bureau of Topographic and Geologic Survey.

Smith, H. T. U., 1953, The Hickory Run boulder field, Carbon County, Pennsylvania: American Journal of Science, v. 251, p. 625-642.

Stone, J., 2000a, Air pressure and cosmogenic isotope production: Journal of Geophysical Research, v. 105, no. b10, p. 23753-23759.

Stone, J. O., 2000b, Cosmogenic isotope constraints on geomorphic processes and landscape evolution: Fission track 2000; 9th international conference on fission track dating and thermochronology Abstracts - Geological Society of Australia, v. 58, p. 309-310.

Wedo, A. M., 2013, Boulder orientation, shape, and age along a transect of the Hickory Run Boulder Field, Pennsylvania [Master of Science in Geography: University of Delaware.

Weissel, J. K., and Seidl, M. A., 1997, Influence of rock strength properties on escarpment retreat across passive continental margins: Geology (Boulder), v. 25, no. 7, p. 631-634.

Weissel, J. K., and Seidl, M. A., 1998, Inland propagation of erosional escarpments and river profile evolution across the southeast Australian passive continental margin: Geophysical Monograph, v. 107, p. 189-206.

West, N., Kirby, E., Bierman, P., and Clarke, B. A., 2014, Aspect-dependent variations in regolith creep revealed by meteoric 10Be: Geology, v. 42, no. 6, p. 507-510.

West, N., Kirby, E., Bierman, P., and Rood, D., 2011, Preliminary estimates of regolith generation and mobility in the Susquehanna Shale Hills Critical Zone Observatory, Pennsylvania, using meteoric 10 Be: Applied Geochemistry, v. 26, p. S146-S148.

West, N., Kirby, E., Bierman, P., Slingerland, R., Ma, L., Rood, D., and Brantley, S., 2013, Regolith production and transport at the Susquehanna Shale Hills Critical Zone Observatory, part 2: insights from meteoric 10Be: Journal of Geophysical Research: Earth Surface, v. 118, no. 3, p. 1877-1896.

Whipple, K., Wobus, C., Crosby, B., Kirby, E., and Sheehan, D., 2007, New tools for quantitative geomorphology: extraction and interpretation of stream profiles from digital topographic data: GSA Short Course, v. 506.

Whipple, K. X., and Tucker, G. E., 1999, Dynamics of the stream‐power river incision model: Implications for height limits of mountain ranges, landscape response timescales, and research needs: Journal of Geophysical Research: Solid Earth, v. 104, no. B8, p. 17661-17674.

Whipple, K. X., and Tucker, G. E., 2002, Implications of sediment-flux-dependent river incision models for landscape evolution: Journal of Geophysical Research, B, Solid Earth and Planets, v. 107, no. 2.

Willenbring, J. K., and Blanckenburg, F. v., 2010, Meteoric cosmogenic Beryllium-10 adsorbed to river sediment and soil: Applications for Earth-surface dynamics: Earth-Science Reviews, v. 98, p. 105-122.

Willett, S. D., McCoy, S. W., Perron, J. T., Goren, L., and Chen, C.-Y., 2014, Dynamic reorganization of river basins: Science, v. 343, no. 6175, p. 1248765.

Wilson, P., Bentley, M. J., Schnabel, C., Clark, R., and Xu, S., 2008, Stone run (block stream) formation in the Falkland Islands over several cold stages, deduced from cosmogenic isotope (10Be and 26Al) surface exposure dating: Journal of Quaternary Science, v. 23, no. 5, p. 461-473.

Wilson, P., Matthews, J. A., and Mourne, R. W., 2016, Relict Blockstreams at Insteheia, Valldalen-Tafjorden, Southern Norway: Their Nature and Schmidt Hammer Exposure Age: Permafrost and Periglacial Processes, v. 28, no. 1, p. 286-297.

Wobus, C., Whipple, K. X., Kirby, E., Snyder, N., Johnson, J., Spyropolou, K., Crosby, B., and Sheehan, D., 2006a, Tectonics from topography: Procedures, promise and pitfalls: Tectonics, climate, and landscape evolution: Geological Society of America Special Paper, v. 398, p. 55–74.

Wobus, C. W., Crosby, B. T., and Whipple, K. X., 2006b, Hanging valleys in fluvial systems: Controls on occurrence and implications for landscape evolution: Journal of Geophysical Research: Earth Surface, v. 111, no. F2, p. n/a-n/a.